Article

Cell Metabolism

System-wide Benefits of Intermeal Fasting by Autophagy

Graphical Abstract

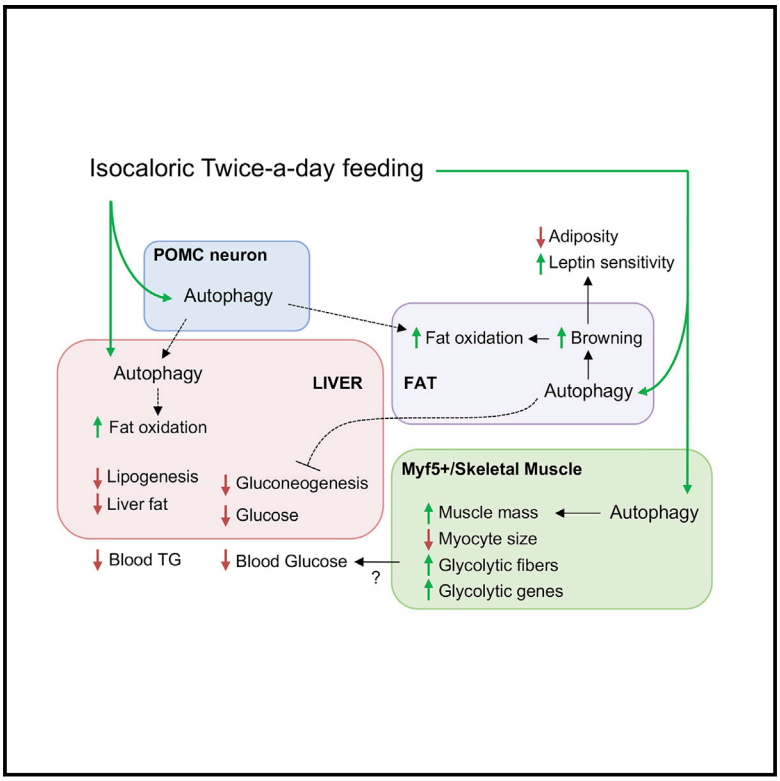

Authors

Nuria Martinez-Lopez, Elena Tarabra, Miriam Toledo, ..., Gary J. Schwartz, Sander Kersten, Rajat Singh

Correspondence

rajat.singh@einstein.yu.edu

In Brief

Our studies suggest that consuming two meals a day with complete food restriction in between the meals is sufficient to lower blood glucose and lipid levels. This simple dietary approach activates a cell "cleansing system" called autophagy in liver, fat, brain, and muscle that helps prevent obesity and diabetes.

Highlights

- Isocaloric twice-a-day (ITAD) feeding impacts autophagy in multiple tissues
- ITAD feeding promotes diverse metabolic benefits in multiple tissue systems
- ITAD feeding prevents age- and obesity-associated metabolic defects
- Tissue-specific autophagy contributes to distinct benefits of ITAD feeding

Martinez-Lopez et al., 2017, Cell Metabolism *26*, 856–871
December 5, 2017
https://doi.org/10.1016/j.cmet.2017.09.020

System-wide Benefits of Intermeal Fasting by Autophagy

Nuria Martinez-Lopez,[1,2,7,8] Elena Tarabra,[1,7] Miriam Toledo,[1,2] Marina Garcia-Macia,[1,2,8] Srabani Sahu,[1,2] Luisa Coletto,[1] Ana Batista-Gonzalez,[1,2] Nir Barzilai,[1,2,5,6] Jeffrey E. Pessin,[1,2,5,6] Gary J. Schwartz,[1,4,5,6] Sander Kersten,[3] and Rajat Singh[1,2,5,6,*]

[1]Department of Medicine, Albert Einstein College of Medicine, 1300 Morris Park Avenue, Forchheimer 505D, Bronx, NY 10461, USA
[2]Department of Molecular Pharmacology, Albert Einstein College of Medicine, Bronx, NY 10461, USA
[3]Division of Human Nutrition, Wageningen University, Wageningen, the Netherlands
[4]Department of Neurology and Neuroscience, Albert Einstein College of Medicine, Bronx, NY 10461, USA
[5]Institute for Aging Research, Albert Einstein College of Medicine, Bronx, NY 10461, USA
[6]Diabetes Research Center, Albert Einstein College of Medicine, Bronx, NY 10461, USA
[7]These authors contributed equally
[8]Present address: Institute for Cell and Molecular Biosciences, Newcastle University, Newcastle Upon Tyne NE4 5PL, UK
*Correspondence: rajat.singh@einstein.yu.edu
https://doi.org/10.1016/j.cmet.2017.09.020

SUMMARY

Autophagy failure is associated with metabolic insufficiency. Although caloric restriction (CR) extends healthspan, its adherence in humans is poor. We established an isocaloric twice-a-day (ITAD) feeding model wherein ITAD-fed mice consume the same food amount as *ad libitum* controls but at two short windows early and late in the diurnal cycle. We hypothesized that ITAD feeding will provide two intervals of intermeal fasting per circadian period and induce autophagy. We show that ITAD feeding modifies circadian autophagy and glucose/lipid metabolism that correlate with feeding-driven changes in circulating insulin. ITAD feeding decreases adiposity and, unlike CR, enhances muscle mass. ITAD feeding drives energy expenditure, lowers lipid levels, suppresses gluconeogenesis, and prevents age/obesity-associated metabolic defects. Using liver-, adipose-, myogenic-, and proopiomelanocortin neuron-specific autophagy-null mice, we mapped the contribution of tissue-specific autophagy to system-wide benefits of ITAD feeding. Our studies suggest that consuming two meals a day without CR could prevent the metabolic syndrome.

INTRODUCTION

Decreased quality control and accumulation of damaged organelles are factors contributing to chronic diseases including the metabolic syndrome. Autophagy, a lysosomal quality control pathway critical for cellular cleanliness, is compromised with age, setting the basis for chronic diseases (Rubinsztein et al., 2011). In fact, mice knocked out (KO) for the autophagy gene *Atg7* or lacking Beclin function display early lethality (Karsli-Uzunbas et al., 2014) and metabolic defects including fat accumulation (Singh et al., 2009a), muscle loss (Martinez-Lopez et al., 2013; Masiero et al., 2009), and glucose intolerance (He et al., 2012; Karsli-Uzunbas et al., 2014).

Caloric restriction (CR) extends healthspan and lifespan in multiple organisms (Colman et al., 2009; Mattison et al., 2012). Despite its remarkable benefits, humans adhere poorly to CR (Moreira et al., 2011), which has motivated the search for sustainable approaches to extend healthspan. Alternate feeding strategies, including intermittent fasting (Anson et al., 2003; Heilbronn et al., 2005; Varady et al., 2009), fasting-mimicking intervention (Brandhorst et al., 2015), and time-restricted feeding (Chaix et al., 2014) each mimic the effects of CR. Since fasting activates autophagy, it is conceivable that dietary interventions mediate their benefits, in part, through autophagy. The integrative physiology of autophagy and its ability to promote metabolic correction in a dietary intervention model remains unexplored.

Because fasting activates autophagy, we established an isocaloric twice-a-day (ITAD) feeding model wherein test mice eat the same amount of food as *ad libitum* (Ad-lib) controls (Con), albeit they eat their food at two 2 hr windows early and late in the diurnal cycle. We hypothesized that adopting the ITAD feeding strategy will eliminate scattered feeding, and provide two windows of intermeal fasting in each circadian period, which in principle will sustain autophagy without the need to restrict calories or alter the type of food consumed. Here we show that ITAD feeding promotes system-wide benefits including reduction of body fat and increased lean mass that accompany significant tissue remodeling. ITAD feeding sustains autophagy levels in aged mice, and prevents age-associated energy imbalance, dyslipidemia, and glucose intolerance. Using liver-, adipose-, myogenic-, and hypothalamic proopiomelanocortin (POMC) neuron-specific *Atg7* KO mice, we identified the contribution of cell-specific autophagy to system-wide benefits of ITAD feeding.

RESULTS

ITAD Feeding in Mice

To develop a feeding strategy that incorporates periods of fasting between feeding windows, we randomized 4-month-old C57BL/6J male mice into Ad-lib Con and ITAD groups. ITAD

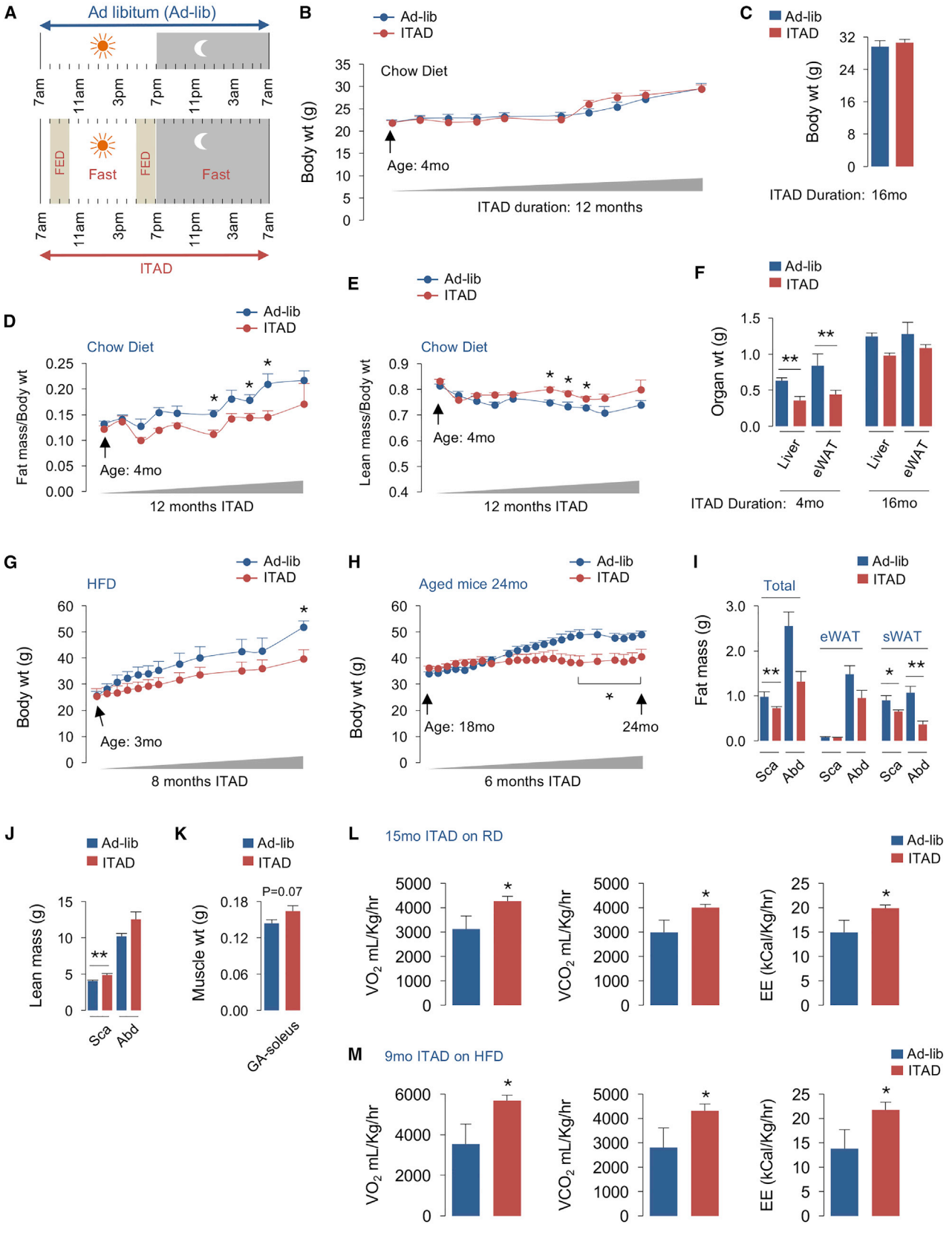

(legend on next page)

mice were fed between 8 and 10 a.m. (feeding window 1) and between 5 and 7 p.m. (feeding window 2), such that food consumed at these two diurnal windows equals the food consumed by Ad-lib mice in 24 hr (Figure 1A). Analyses of food consumed per cage revealed that test mice (5 mice per cage) acclimatized to ITAD feeding by day 6, indicated by progressive increases in cumulative chow intake in the two windows (Figure S1A, lower panel). Thereafter, we noted that each cage of five mice consumed the same amount of food per day (Ad-lib versus ITAD; 15.1 ± 0.7 g/cage/day versus 14.9 ± 0.8 g/cage/day) (Figures S1A and S1B). After 16 months, both groups had consumed similar amounts of regular chow diet (RD) (Ad-lib cage versus ITAD cage; 7,109 versus 6,975 g) (Figure S1C). Similarly, test mice (5 mice per cage) fed high-fat diet (HFD; 60% calories in fat) acclimatized to ITAD feeding by day 3 (Ad-lib versus ITAD; 8.95 ± 0.6 g/cage/day versus 8.77 ± 0.6 g/cage/day) (Figures S1D and S1E). After 8 months, Con and ITAD groups had consumed similar amounts of HFD (Ad-lib cage versus ITAD cage; 2,077 versus 2,035 g) (Figure S1F). Our goal was to establish diurnal ITAD feeding and nocturnal isocaloric twice-a-night (ITAN) feeding strategies and compare their abilities to induce autophagy and prevent metabolic syndrome. Since ITAD and ITAN feeding led to similar effects on body weight in RD-fed mice, we pursued our long-term feeding studies in ITAD-fed mice.

ITAD Feeding Influences Body Composition and Energy Expenditure

Monthly body weight (wt) analyses for 12 months, and at 16 months of ITAD feeding, revealed no differences between RD-fed Ad-lib and ITAD mice, supporting similar caloric intake by both groups (Figures 1B and 1C). However, quantitative nuclear magnetic resonance (qNMR) analyses revealed progressive loss of body fat and proportionate increase in lean mass as early as 3 months of ITAD feeding (Figures 1D and 1E), indicating that partitioning calories into two meals is sufficient to alter body composition. In fact, analysis of tissue wt from RD-fed mice subjected to ITAD feeding for 4 months showed significantly decreased liver and epididymal white adipose tissue (eWAT) wt (Figure 1F) in absence of changes in body wt (Figures 1B and 1C). However, after 16 months of ITAD feeding, decreases in liver and eWAT wt did not acquire statistical significance (Figure 1F). By contrast, 3-month-old (Figure 1G) and 18-month-old (Figure 1H) mice subjected to ITAD feeding on HFD for 8 and 6 months, respectively, resisted wt gain compared with Con mice.

To determine whether ITAD feeding increased muscle mass, we subjected mice to X-ray computed tomography (CT). CT reconstructions confirmed that ITAD feeding on RD for 12 months reduced total fat mass and decreased subcutaneous WAT (sWAT) mass in abdominal (Abd) and scapular (Sca) planes (Figure 1I). Further, CT revealed a trend of reduced eWAT mass in the Abd plane (Figure 1I). CT also showed a significant increase in lean mass in the Sca plane and a trend for the same in the Abd plane of ITAD-fed mice compared with Con (Figure 1J). Consistent with increased lean mass, gastrocnemius/soleus (GA-sol) muscles from 12-month-old ITAD mice weighed modestly more than those in Con (Figure 1K). Reduction of fat mass in ITAD mice was associated with increased oxygen consumption (VO2), carbon dioxide production (VCO2), and energy expenditure (EE) (Figures 1L, 1M, S1G, and S1H), which did not result from increased locomotion (Figures S1I and S1J). Thus, ITAD feeding normalizes age- and diet-associated energy imbalance.

ITAD Feeding Impacts Circadian Autophagy

Because ITAD feeding provides two periods of intermeal fasting, which activates autophagy, we tested if and when ITAD feeding stimulates autophagy. Our initial qPCR analyses at six time points across 24 hr (7 a.m., 11 a.m., 3 p.m., 7 p.m., 11 p.m., and 3 a.m.) revealed modest increases in expression of autophagy-related genes *Lc3* (light chain 3) and *Beclin1* during the first feeding window in ITAD-fed mice (data not shown). Consequently, we comprehensively tested the effect of ITAD feeding on autophagy activity across 24 hr via LC3-II flux analyses in livers exposed or not to lysosomal inhibitors at each of the six time points. LC3-II flux analyses from distinct pools of mice subjected to ITAD feeding for 8–10 months revealed progressive increases in autophagy from 7 to 11 a.m. and maintenance of flux until 2 p.m., following which autophagy flux steadily declined until 7 p.m. to levels lower than those in Ad-lib mice (Figures 2A and S2A). After 7 p.m., LC3-II flux gradually increased to reach its zenith at 3 a.m. in IT AD-fed mice (Figure 2A). Upon comparing the oscillations of LC3-II flux in both groups (Figure 2A), we noted a clear shift in phase of autophagy flux in ITAD-fed mice characterized by 8–10 a.m. feeding-associated induction of autophagy, a clear departure from the typical increase in autophagy during starvation. Consistent with maximal autophagy flux at 11 a.m., *Atg* gene expression was increased in GA (Figure 2B), iWAT (Figure 2C), and mediobasal hypothalamus (MBH) (Figure S2B) at 11 a.m. after as early as 4 months of ITAD feeding. Beclin1 protein levels were also increased to varying degrees at 11 a.m. in several tissues from 4 month ITAD-fed mice (Figure 2D). Tissue-wide autophagy flux analyses revealed ~2.5-fold increase in flux of autophagy cargo p62 in MBH, ~3-fold increase in LC3-II flux in brown adipose tissue, and ~2-fold increase in LC3-II flux in GA at 11 a.m. from mice subjected to ITAD feeding for 8 months (Figures 2E–2G).

Figure 1. ITAD Feeding Influences Body Composition and Energy Expenditure

(A–F) The isocaloric twice-a-day feeding (ITAD) strategy wherein test mice feed between 8 and 10 a.m. and between 5 and 7 p.m. the same amount of food that *ad libitum* (Ad-lib)-fed controls (Con) eat in 24 hr (A). Body weight (wt) (B and C), body composition (D and E), and tissue wt (F) at indicated intervals in regular chow diet (RD)-fed male mice subjected to Ad-lib or ITAD feeding for indicated duration (n = 5).

(G and H) Body wt of young (G) and aged (H) male mice fed Ad-lib or ITAD on a high-fat diet (HFD) for indicated durations (n = 5).

(I and J) CT for total fat or fat distributed in epididymal (eWAT) or subcutaneous (sWAT) pads (I) and CT for lean mass in scapular (Sca) and abdominal (Abd) planes in Ad-lib or ITAD-fed male mice on RD for 12 months (mo) (J) (n = 5).

(K) Gastrocnemius (GA) and soleus muscle wt in RD-fed male mice on Ad-lib or ITAD for 12 months (n = 5).

(L and M) VO2, VCO2, and EE rates in male mice fed Ad-lib or ITAD on RD (L) or HFD for the indicated duration (M) (n = 5).

Bars are mean ± SEM. *$p < 0.05$, **$p < 0.01$. Student's t test or two-factor ANOVA and Bonferroni correction. See also Figure S1.

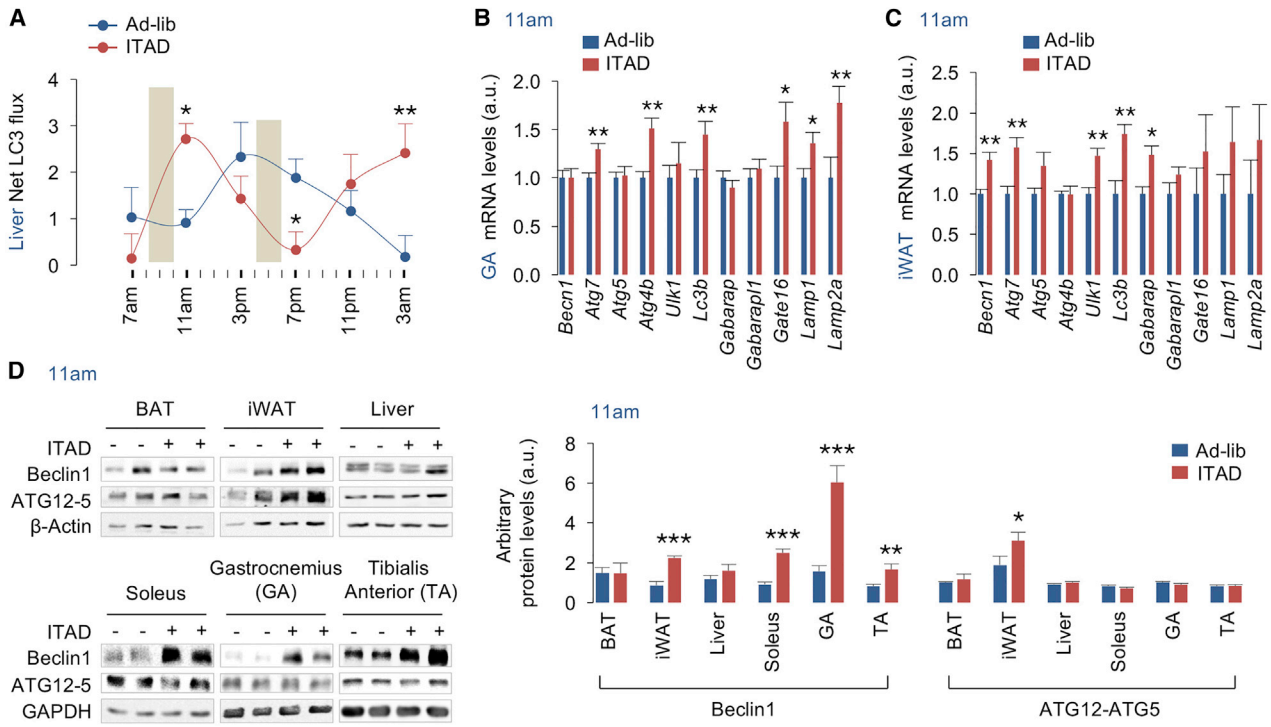

(legend on next page)

Since mechanistic target of rapamycin (mTOR) and AMP-regulated kinase (AMPK) (Egan et al., 2011) regulate autophagy, we examined how their activities correlated with changes in LC3-II flux across 24 hr. Immunoblotting of liver lysates revealed that increases in LC3-II flux at 11 a.m. from ITAD mice were associated with significantly increased phosphorylated (P)-AMPK levels (Figures S2C and S2D). AMPK is induced by starvation, yet, surprisingly, we noted increased P-AMPK levels in the 8–10 a.m. feeding window in ITAD mice, suggesting that autophagy induction is perhaps AMPK driven. ITAD feeding also increased P-S6 levels in both feeding windows reflecting nutrient-driven mTOR complex 1 activity (Figures S2E and S2F). Indeed, recent work has shown that availability of nutrients concurrently activates AMPK and mTOR (Dalle Pezze et al., 2016). Since mTOR suppresses autophagy, and because autophagy is active between 7 and 11 a.m. in ITAD mice (Figure 2A), mTOR signaling at 11 a.m. is likely uncoupled from autophagy as demonstrated in secretory cells (Narita et al., 2011).

Because lipophagy (Singh et al., 2009a) drives fat utilization and oxygen consumption rates (OCRs) (Martinez-Lopez et al., 2016), autophagy activation at 11 a.m. in ITAD-fed mice was associated with ~2-fold increase in hepatic OCRs (Figure 2H), while suppression of LC3-II flux at 7 p.m. (Figures 2I and 2A) was associated with normalization of OCRs to basal rates (Figure 2J). Our studies do not reveal the mechanism for time-dependent modulation of autophagy in ITAD-fed mice; however, it is likely that complex interplay between AMPK, a regulator of the circadian clock (Lamia et al., 2009) and autophagy (Egan et al., 2011); mTOR; and possibly a subset of core circadian proteins differentially regulates autophagy at distinct time points during ITAD feeding.

ITAD Feeding Promotes iWAT Browning

Since ITAD feeding decreases fat mass, we characterized the effect of ITAD feeding on WAT. Consistent with reduced fat mass, ITAD-fed mice displayed reduced serum leptin levels, with values displaying statistical significance at 7 a.m. and 11 p.m., indicating improved leptin sensitivity (Figure S3A). Hematoxylin and eosin (H&E) stains of WAT revealed decreased adipocyte size in ITAD-fed mice (Figure 3A), which in conjunction with increased EE (Figures 1L and 1M) suggested increased fat utilization. Indeed, iWAT from ITAD mice displayed pockets of uncoupling protein 1 (UCP1)-positive brown adipocytes displaying multiloculated lipid droplets (LDs) (Figures 3A–3C and S3B). Increased expression of brown genes *Zic1*, *Eva1*, and *Fbxo31* in iWAT, and no changes in expression of beige genes *Tmem26*, *Klhl13*, and *Tbx1* (Wu et al., 2012), supported iWAT browning in ITAD-fed mice (Figure 3D). We also noted an ~3-fold increase in expression of adipogenic precursor *Ebf2* (Rajakumari et al., 2013) and *Pdgfr*α (Berry and Rodeheffer, 2013) in iWAT from ITAD mice (Figure 3E). Since *Ebf2* determines brown adipocyte identity, we suspect that *Ebf2* orchestrates iWAT browning in ITAD mice. Although we detected a statistically insignificant increase in expression of myogenic factor *Myf5* in eWAT from ITAD mice (Figure 3E), the significance of this increase is unclear. In keeping with increased mitochondrial mass in brown adipocytes, we noted significant increases in expression of mitochondrial markers *Cpt1b* and *Cox4* and of *Pgc1*α, a driver of mitochondrial biogenesis, in iWAT, and ~1.5- to 2-fold increase in expression of adipogenic factor *Ppar*γ in iWAT and eWAT (Figure 3F). Consistent with these data, respirometry revealed an ~2-fold increase in OCRs in iWAT ($p = 0.07$) (Figure 3G), but not in eWAT (Figure 3H). Further, ITAD feeding improved the ability to respond to cold (4°C for 1 hr), indicated by increased expression of brown fat genes, but not beige genes, in iWAT (Figure 3I).

ITAD Feeding Increases M2 Macrophage Markers in eWAT

Surprisingly, ITAD feeding increased F4/80 positivity in WAT, indicating macrophage infiltration (Figure S3C). Because alternatively activated M2 macrophages are anti-inflammatory in nature (Bouhlel et al., 2007), we tested whether increased F4/80 positivity reflected an increase in M2 macrophage content. Indeed, qPCR analyses in eWAT, a fat depot prone to inflammation, revealed remarkably increased anti-inflammatory M2 macrophage markers *Arg1* (~4-fold), *Ym1* (~2-fold), and *IL-10* (~2-fold) in ITAD-fed mice, while only a modest increase in pro-inflammatory *IL-6* expression was observed (Figure 3J). By contrast, expression of anti- or pro-inflammatory cytokine genes remained unremarkable in iWAT (Figure 3J).

ITAD Feeding Increases Type IIB Fibers in Skeletal Muscle

To understand how ITAD feeding increases muscle mass (Figures 1K and S3D), we examined the effect of ITAD feeding on myocyte proliferation and fiber-type changes. H&E-stained GA from ITAD-fed mice for 9–10 months revealed myocytes that were ~25% smaller in size than Con mice (Figures 3K and S3E). In fact, we noted an abundance of myocytes with cross-sectional area 5,000–15,000 pixel^2 on a scale from 0 to 40,000 pixel^2 (Figure 3L). ITAD feeding also increased the number of cells with centralized nuclei (Figures 3K and 3M). Small myocytes with centralized nuclei reflect proliferating and regenerating muscle (Charge and Rudnicki, 2004). Accordingly, we noted an ~30%–40% increase in expression of myogenic factors *Myf5*, *Myf6*, and *Myog* without changes in *Myod1* and *Ckm* expression

Figure 2. ITAD Feeding Impacts Autophagy Flux

(A) Net LC3-II flux across 24 hr in liver explants from male mice in presence or absence of lysosomal inhibitors (Lys Inh) from RD-fed mice on Ad-lib or ITAD feeding for 8–10 months. Representative blots shown in Figure S2A ($n = 6$).

(B–D) qPCR for indicated autophagy and lysosomal genes in gastrocnemius (GA) and iWAT ($n = 8$) (B and C) and immunoblots (IB) for Beclin1 and ATG12-ATG5 conjugate in the indicated tissues harvested at 11 a.m. from RD-fed male ($n = 4$) and female mice ($n = 4$) on Ad-lib or ITAD feeding for 4 months (total $n = 8$) (D). Densitometry values in (D) are shown (right).

(E–G) IB for p62 or LC3 depicting autophagy flux in explants from MBH (mediobasal hypothalamus), BAT, and GA treated (+) or not (−) with Lys Inh from RD-fed male ($n = 4$) and female mice ($n = 4$) on Ad-lib or ITAD for 8 months (total $n = 8$). Quantifications for net p62 or LC3-II flux are shown.

(H–J) Oxygen consumption rates (OCRs) in livers at 11 a.m. (H), IB for LC3 in livers at 7 p.m. and treated (+) or not (−) with Lys Inh for 2 hr (I), and OCR in livers at 7 p.m. from RD-fed male mice on Ad-lib or ITAD for 10 months (J) ($n = 3$). Quantification for net LC3-II flux and steady-state LC3-II are shown.

Bars are mean ± SEM. *$p < 0.05$, **$p < 0.01$, ***$p < 0.001$. Student's t test or two-factor ANOVA and Bonferroni correction. See also Figure S2.

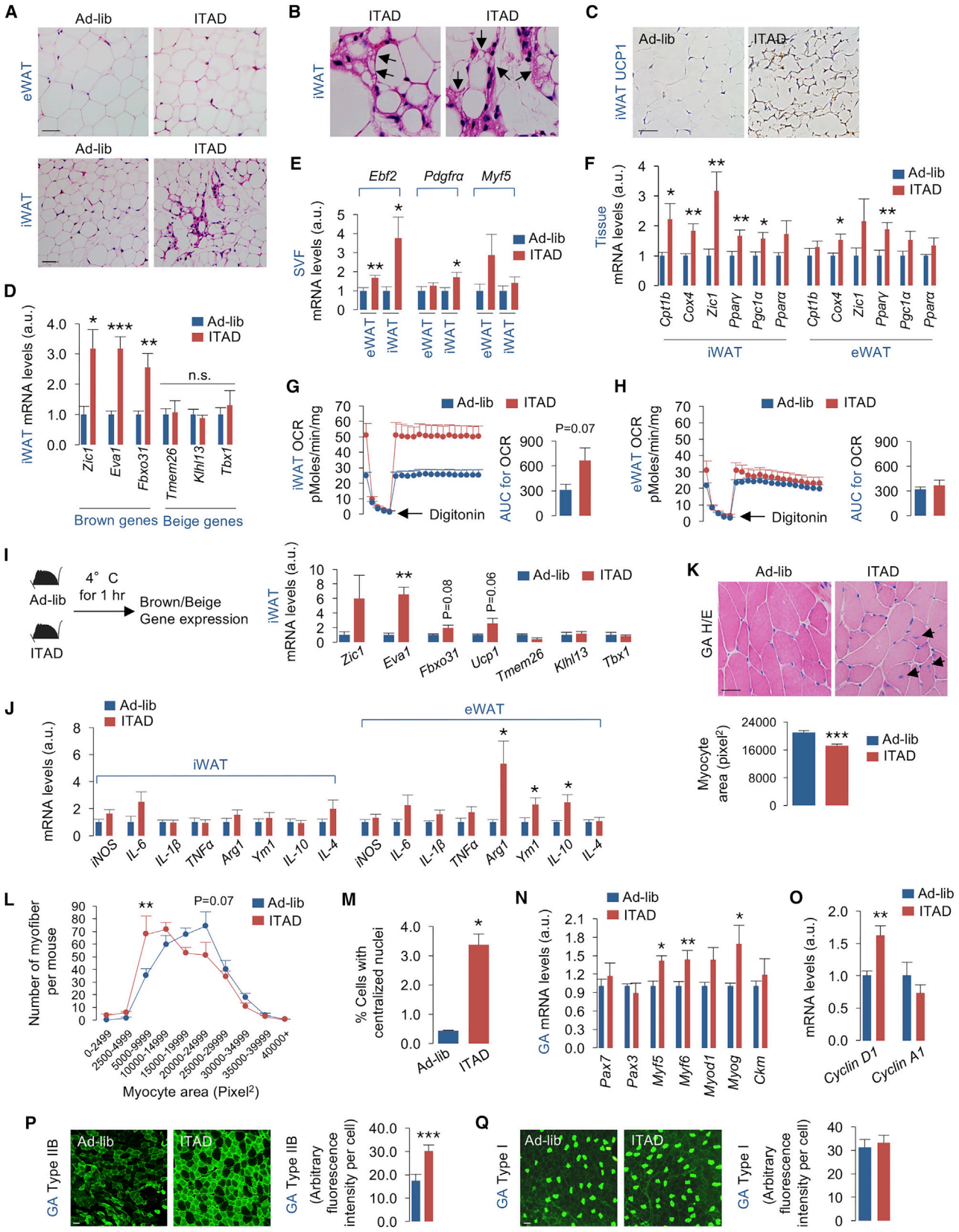

(legend on next page)

(Figure 3N), and an ~1.6-fold increase in expression of proliferation marker Cyclin D1 (Figure 3O), indicating active myogenesis in ITAD-fed mice.

Since aging is associated with preferential loss of type IIB glycolytic fibers (Marzetti et al., 2009), we investigated the effect of ITAD feeding on type IIB fiber content. Staining for myosin heavy chain (MyHC) glycolytic type IIB and oxidative type I fibers in GA from 10-month-old ITAD-fed mice (analyzed at 14 months of age) revealed a remarkable increase in type IIB fibers without changes in type I fiber content, indicating glycolytic fiber expansion (Figures 3P and 3Q). Since increased glycolytic fiber number is associated with reduced endurance, we tested the effect of ITAD feeding on exercise capacity. During 3 days of acclimatization on a treadmill-based exercise regime (Figures S3F and S3G) (He et al., 2012), we failed to observe significant differences in exercise capacities by both groups. During the test (Figure S3H), when treadmill speed was increased by 1 m/min every min, consistent with increased type IIB fiber content, ITAD-fed mice fatigued earlier at 28 m/min speed, indicated by increased shocks required to stay on the treadmill. Nevertheless, ITAD feeding leads to retention of key attributes of skeletal muscle that are typically lost with age: mass and type IIB fiber content.

ITAD Feeding Suppresses Hepatic Gluconeogenesis

To explore the effect of ITAD feeding on glucose/lipid metabolism, we characterized circulating insulin/glucose levels, liver/serum triglycerides (TGs), and expression of glucose/lipid metabolism genes in livers from Ad-lib and ITAD-fed mice across 24 hr. Surprisingly, ITAD-fed mice displayed a surge in serum insulin levels that correlated with 5–7 p.m. feeding (Figure 4A), after which insulin levels dropped to levels lower than those in Ad-lib mice. Increased serum insulin at 7 p.m. in ITAD-fed mice was associated with reduced blood glucose levels from 7 p.m. to 3 a.m. (Figure 4B), suggesting that 7 p.m. insulin release possibly increased tissue glucose uptake and/or suppressed gluconeogenesis. Supporting the latter, livers from ITAD-fed mice displayed varying degrees of reduction in expression of gluconeogenic genes *G6pc*, *Pck1*, and *Fbp1* at 7 p.m. compared with Con (Figures 4C, S4A, and S4B). Pyruvate tolerance tests (PTTs) initiated at 6 p.m. in mice food deprived from 10 a.m. onward and fed for 10 min at 5 p.m. (Figure 4D) displayed reduced blood glucose levels in ITAD mice (Figure 4E), confirming decreased gluconeogenesis. Although we cannot explain the reason for increased serum insulin at 7 p.m. (and not after the first feeding window), it is likely that insulin's ability to suppress autophagy inhibited autophagy flux at 7 p.m. in ITAD mice (Figures 2A and 2I).

Active Lipophagy and Reduced Lipogenesis in Livers from ITAD Mice

Liver TG analyses revealed significantly decreased lipid levels in ITAD-fed mice (Figure 4F), while serum TGs were only modestly lower in ITAD-fed mice on RD (Figure 4G). Increases in autophagy flux and OCR in liver at 11 a.m. (Figures 2A and 2H) correlated with ~3-fold increase in *Pparα* expression at 11 a.m. (Figure 4H), a key driver of autophagy (Lee et al., 2014), suggesting a role for lipophagy in ITAD feeding-driven liver TG depletion (Figure 4F). At 11 a.m., we also noted increased expression of *Pparα* target *Fgf21*, and a trend toward increased FGF21 secretion (Figures 4I and 4J) (Badman et al., 2007; Inagaki et al., 2007), which may have contributed to liver fat loss. Quite surprisingly, qPCR analyses for *Srebp1c*, the master regulator of lipogenesis, and its targets *Fas*, *Elovl6*, *Acsl5*, and *Gpat1*, indicated maximal suppression of lipogenesis in ITAD mice at 7 p.m. (Figures 4K–4O). Since autophagy flux and OCR were suppressed from 3 to 11 p.m. (Figures 2A, 2I, and 2J), decreased liver TG after 7 p.m. in ITAD-fed mice (Figure 4F) may have resulted from suppressed lipogenesis despite the surge in serum insulin, a key driver of TG synthesis. These results suggest that induction of lipophagy (11 a.m.) and suppression of lipogenesis (7 p.m.) act in concert to limit hepatic TG accumulation in ITAD-fed mice (Figure 4P).

ITAD or ITAN (Nocturnal) Feeding Has Distinct Benefits in Young Chow-Fed Mice

Restricted feeding uncouples peripheral clocks from the light-entrained central clock (Damiola et al., 2000), suggesting that changes in peripheral clocks may contribute to the phenotype of ITAD-fed mice. In fact, analyses of oscillations of core clock genes in livers from ITAD-fed mice revealed a modest, albeit statistically insignificant, increase in expression of circadian driver *Bmal1* (Figure S4C). We also noted changes in oscillations of clock repressors *Per1*, *Per2*, and *Per3*, with shifts in phase in expression of *Per1* and *Per3* (Figures S4C–S4H). Given the role of circadian proteins in metabolic regulation (Bass and Takahashi, 2010), it is likely that diurnal ITAD feeding, and resulting changes in expression of clock genes, shapes the phenotype of ITAD-fed mice. To explore this possibility, we compared changes in body wt, eWAT wt, iWAT browning, and iWAT OCR in mice fed ITAD or ITAN (fed at 8–10 p.m. and 5–7 a.m.) on RD (Figure S5A). After 4 months, we noted no difference in

Figure 3. ITAD Feeding Remodels Adipose Tissue and Skeletal Muscle

(A–C) H&E-stained fat tissues (arrows show multiloculated adipocytes) (A and B) and UCP1 positivity in iWAT from RD-fed male mice on Ad-lib or ITAD feeding for 4 months (C) (n = 3).

(D–H) qPCR for brown and beige genes (D), adipocyte/myogenic progenitor genes in stromal vascular fractions (SVF) (E), and mitochondrial genes from male (n = 4) and female (n = 4) mice (total n = 8) (F), and OCR and AUC (area under curve) in iWAT and/or eWAT (n = 3) from RD-fed male mice on Ad-lib or ITAD for 12 months (G and H). n.s., not significant.

(I) Experimental plan and qPCR of brown and beige genes in iWAT from RD-fed male mice on Ad-lib or ITAD for 12 months and then exposed to 4°C for 1 hr (n = 3).

(J) Immune markers in iWAT and eWAT from RD-fed male (n = 4) and female mice (n = 4) on Ad-lib or ITAD for 12 months (total n = 8).

(K–M) H&E stains and quantification for myocyte area (K) and distribution of myocytes by area (pixel^2) (L), and percentage of myofibers with centralized nuclei in GA from RD-fed male mice on Ad-lib or ITAD for 10 months (M) (n = 4). Arrows in (K) indicate centralized nuclei.

(N and O) Myogenic genes (N) (n = 10) and cell-cycle genes in GA from RD-fed male mice on Ad-lib or ITAD for 6 months (O) (n = 8).

(P and Q) Immunofluorescence (IF) of type IIB, and type I fibers in GA from RD-fed male mice on Ad-lib or ITAD for 10 months (n = 4).

Bars are mean ± SEM. *p < 0.05, **p < 0.01, ***p < 0.001. Student's t test or two-factor ANOVA and Bonferroni correction. Scale bars, 50 μm. See also Figure S3.

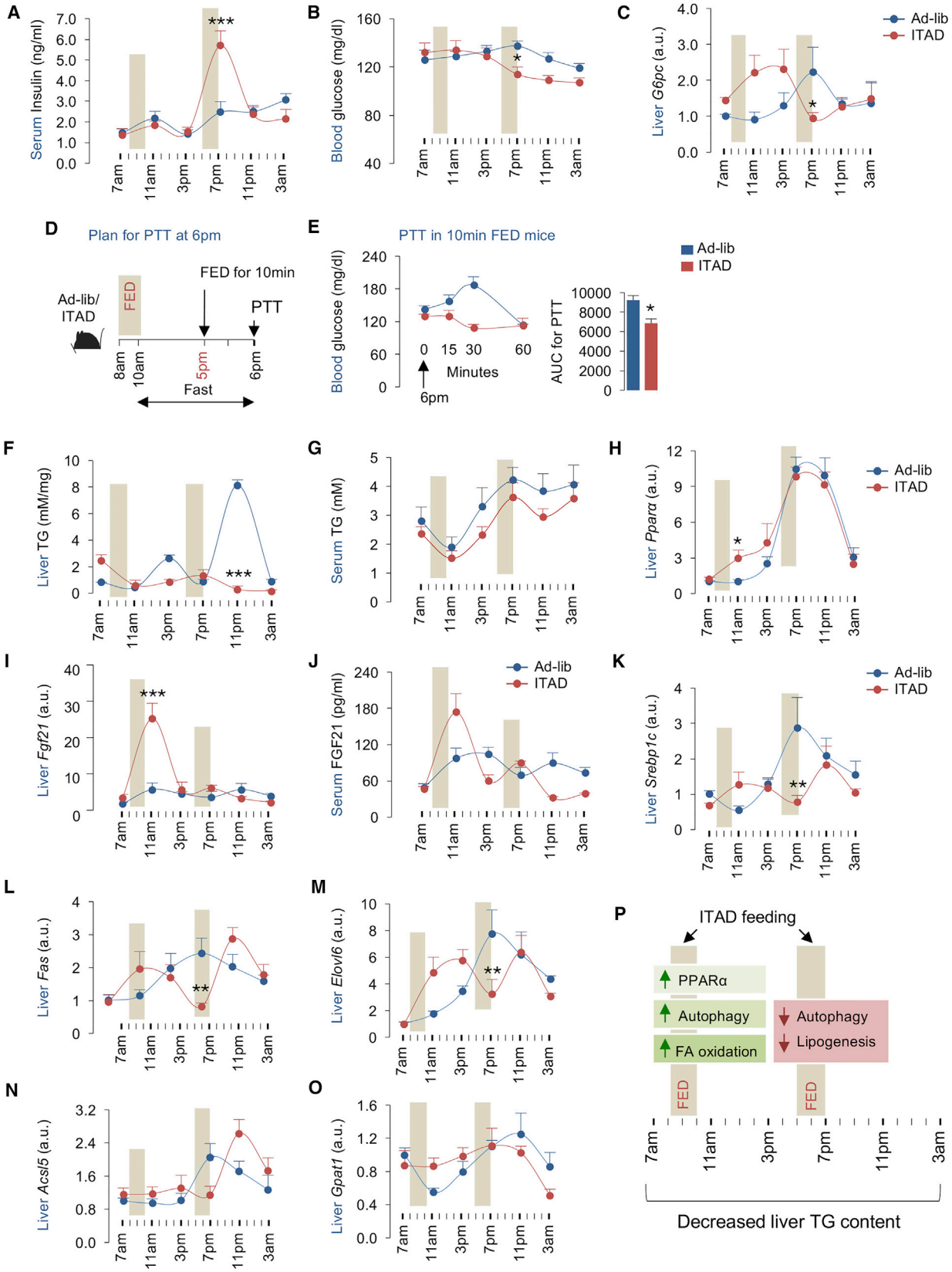

(legend on next page)

body wt between both groups (Figure S5B), although ITAN-fed mice displayed significantly increased eWAT wt (Ad-lib versus ITAN eWAT wt/body wt; 14.0 ± 0.9 versus 19.2 ± 0.8; $p < 0.05$, t test), while ITAD-fed mice showed reduced eWAT wt when compared with Con (Ad-lib versus ITAD eWAT wt/body wt; 16.1 ± 1.1 versus 14.1 ± 0.4; $p < 0.05$, t test). ITAD-fed mice also showed an increase in expression of brown fat marker *Eva1* in iWAT (Figure S5C) that was associated with increased OCR (Figure S5D). ITAN-fed mice displayed similar trends for *Eva1* expression and iWAT OCR, although these values did not acquire statistical significance (Figures S5C and S5D). Strikingly, improvement in glucose clearance occurred earlier in ITAN-fed mice than ITAD-fed mice after 4 months on RD (Figure S5E), suggesting that ITAD or ITAN feeding of young (8 months old) RD-fed mice each leads to distinct metabolic benefits.

ITAD Feeding Prevents Age-Associated Metabolic Defects

To determine whether ITAD feeding prevents age/obesity-associated metabolic compromise, we subjected 4- and 18-month-old mice to Ad-lib or ITAD feeding on HFD for 6 months (Figure 5A). ITAD feeding significantly reduced body wt in 10- (data not shown) and 24-month-old mice (Figure 1H), and reduced fat mass and increased lean mass in 10-month-old mice (Figure 5B), while similar statistically insignificant trends were observed in 24-month-old mice (Figure 5B). ITAD feeding significantly decreased liver wt in young and aged mice (Figure 5C), and reduced liver and serum TG in 10-month-old mice (Figures 5D and 5E), while a trend for decreased liver TG was noted in 24-month-old mice (Figure 5D). Consistent with qNMR data (Figure 5B), ITAD feeding significantly increased GA-sol wt in 10-month-old mice, while modestly increasing GA-sol wt in 24-month-old mice (Figure 5F). ITAD feeding also reversed hypertriglyceridemia by ~50% when mice fed HFD Ad-lib for 8 months were switched to ITAD feeding for 4 months (Figure 5G), indicating that ITAD feeding can reduce hyperlipidemia and potentially lower cardiovascular disease risk.

Since ITAD feeding increases EE, we tested its ability to restore EE in aged mice. Indeed, ITAD feeding prevented age-associated loss of VO2, VCO2, and EE rates (Figures 5H–5J), without changing locomotor activity (Figure 5K). *Seahorse* respirometry (Figure 5L) revealed patterns of increased liver OCR in ITAD-fed aged mice, which were supported by increases in VO2 (Figure 5H). Prevention of age-associated loss of OCR was associated with increased expression of mitochondrial genes *Cox4* and *Cpt2*, and induction of *Pgc1α*, in ITAD-fed aged mice (Figure 5M). ITAD feeding also prevented age-associated reduction in expression of *Atg* genes and lysosomal *Lamp1* (Figure 5N), and increased LC3-II flux in aged livers at 11 a.m. (Figure 5O). Finally, ITAD feeding improved glucose clearance in aged or obese mice subjected to glucose tolerance tests (GTTs) (Figures 5P and 5Q), validating its effectiveness in preventing age/obesity-associated metabolic compromise.

POMCergic Autophagy Controls Lipohomeostasis in ITAD-Fed Mice

Since ITAD feeding activates autophagy in liver, MBH, WAT, and muscle at 11 a.m., we sought to map the contribution of autophagy in each tissue system to metabolic benefits of ITAD feeding. POMCergic autophagy plays crucial roles in regulation of body wt (Coupe et al., 2012; Kaushik et al., 2012; Quan et al., 2012) and fat utilization in peripheral tissues (Martinez-Lopez et al., 2016). Consequently, we asked to what extent is POMCergic autophagy required for benefits of ITAD feeding. To that end, body wt analyses revealed that, while Con mice lost ~20% of their body wt after 4 months of ITAD feeding on HFD, ITAD-fed mice lacking *Atg7* in POMC neurons (*Atg7*KO^{POMC}) resisted losing their body wt (Figure 6A). Further, while ITAD-fed Con mice on HFD decreased their eWAT wt by ~40%, ITAD-fed KO mice maintained their eWAT mass (Figure 6B). In fact, ITAD-fed KO mice failed to induce their iWAT OCR to levels observed in ITAD-fed Con (Figure 6C), possibly due to the reported loss of WAT sympathetic tone in *Atg7*KO^{POMC} mice (Kaushik et al., 2012). ITAD-fed *Atg7*KO^{POMC} mice also resisted lowering their liver and serum TG levels compared with ITAD-fed Con mice (Figures 6D and 6E). To exclude that loss of *Atg7* in POMC neurons from birth led to developmental defects in the hypothalamus, which, in turn, reduced the benefits of ITAD feeding, we generated *Atg7*KO$^{POMC-ERT2Cre}$ mice wherein *Atg7* was deleted during adulthood via tamoxifen (Tmx)-driven expression of *Cre* in POMC neurons (Berglund et al., 2013). As anticipated, 6 weeks of ITAD feeding on HFD significantly decreased serum TG levels in Con and *Atg7*KO$^{POMC-ERT2Cre}$ mice prior to administration of Tmx (i.e., day 0) (Figure 6F). Con and *Atg7*KO$^{POMC-ERT2Cre}$ mice were then subjected to Tmx injections (day 1) and serum TG levels were analyzed on day 15. While Tmx-injected control mice maintained reduced serum TG levels, Tmx-injected *Atg7*KO$^{POMC-ERT2Cre}$ mice lost their ability to lower their serum TG levels in response to ITAD feeding (Figure 6F). Despite these defects in lipid metabolism in *Atg7*KO^{POMC} mice, ITAD-fed Con and *Atg7*KO^{POMC} mice each reduced their glucose production to similar levels in intraperitoneal (i.p.) PTT (Figure S6A), and, accordingly, each displayed equivalent improvements in glucose clearance when subjected to i.p. GTT (Figure S6B). These data show that POMCergic autophagy is required to mediate the effects of ITAD feeding on lipohomeostasis in liver and iWAT, but not glucose homeostasis.

Roles of Autophagy in Hepatic Lipohomeostasis in ITAD-Fed Mice

Because POMCergic autophagy drives hepatic lipophagy in a cell-nonautonomous manner (Martinez-Lopez et al., 2016), we

Figure 4. ITAD Feeding and Glucose and Fat Metabolism in Liver

(A–O) Serum insulin (A) (n = 8), blood glucose levels (B) (n = 14), hepatic gluconeogenic gene *Pck1* at indicated time points (C) (n = 8), pyruvate tolerance test (PTT) at 6 p.m. (D and E) (n = 4), liver and serum TG (F and G) (n = 8), qPCR for hepatic *Pparα* and *Fgf21* genes (H and I) (n = 8), serum FGF21 levels (J) (n = 3), and qPCR for lipogenic genes at indicated time points in male mice subjected to Ad-lib or ITAD feeding on RD for 10 months (K–O) (n = 8).

(P) Summary of effects of ITAD feeding on hepatic lipid metabolism across 24 hr.

Bars are mean ± SEM. *$p < 0.05$, **$p < 0.01$, ***$p < 0.001$. Student's t test or two-factor ANOVA and Bonferroni correction. See also Figure S4.

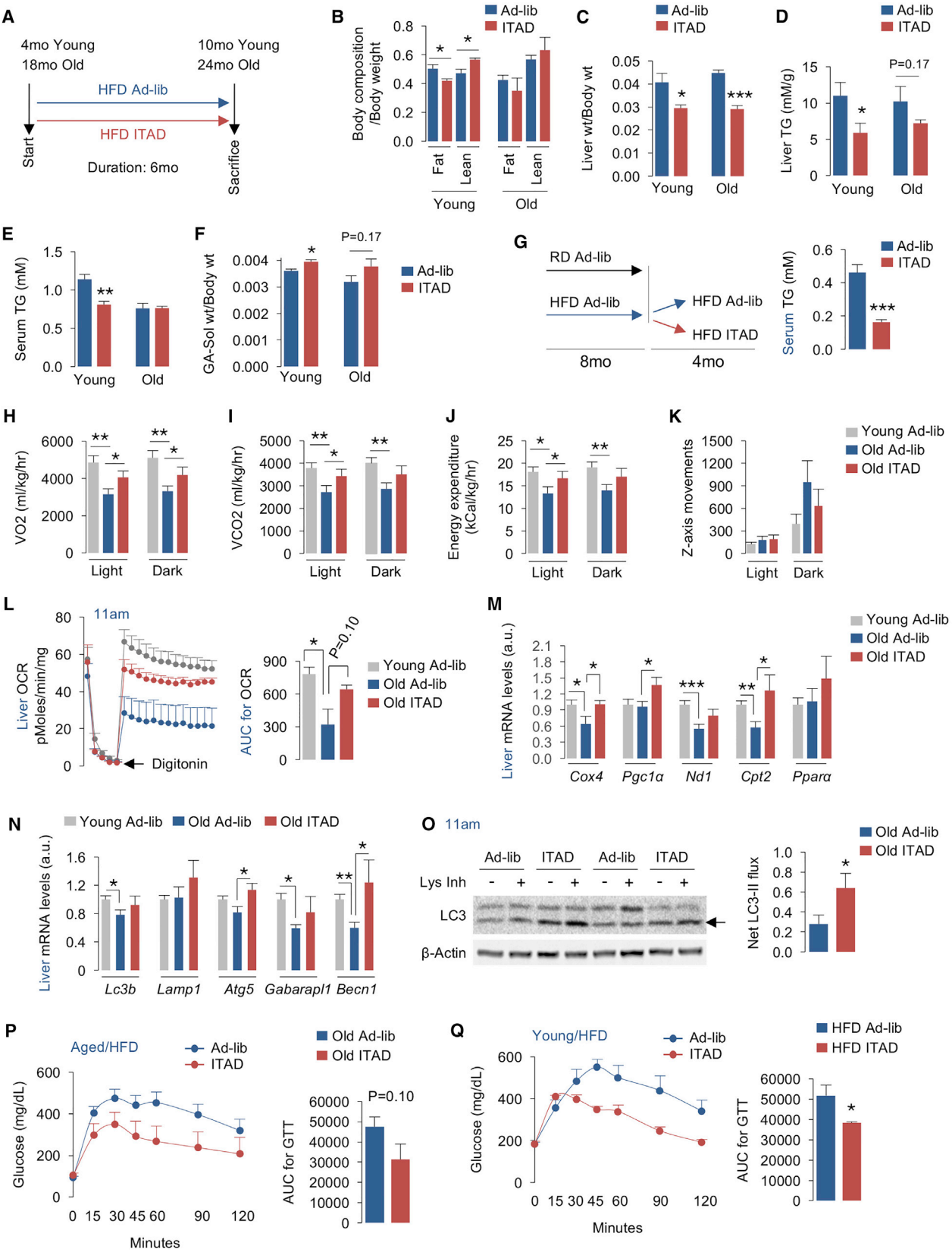

(legend on next page)

investigated the role of POMCergic autophagy in hepatic lysosomal degradation of LD in ITAD mice at 11 a.m. Consistent with increased autophagy flux and OCR at 11 a.m. (Figures 2A and 2H), lysosomal inhibition with i.p. leupeptin (plan in Figure S6C, left) for 2 hr in ITAD-fed Con mice led to ~3-fold increase in liver TGs, indicating lysosomal turnover of TGs at 11 a.m. (Figure S6C, right). By contrast, livers from ITAD-fed *Atg7*KO^{POMC} mice displayed higher basal TG levels, which failed to accumulate upon lysosomal inhibition (Figure S6C), indicating that POMCergic autophagy is required for lipophagy of liver TG in ITAD-fed mice at 11 a.m. In fact, acutely depleting liver *Atg7* by injecting *Cre*-expressing adenoviruses in *Atg7*$^{flox/flox}$ mice or denervating the liver via vagotomy to uncouple the liver from CNS each blocked ITAD feeding-driven increases in liver OCR at 11 a.m. (Figure 6G), demonstrating that POMCergic and liver autophagy act in concert to mobilize lipid in ITAD mice.

Surprisingly, depleting *Atg7* in liver suggests multiple roles of autophagy in decreasing liver TG in ITAD-fed mice. As noted earlier, ITAD feeding suppressed the expression of lipogenic genes, e.g., *Fas* (Figure 4L), and increased expression of *Pgc1α*, *Pparα*, and *Pparα* target *Fgf21* (Figures 6H and 4I), which drive fat oxidation. Intriguingly, depleting *Atg7* in liver reversed ITAD feeding-driven suppression of *Fas* expression, suggesting that autophagy is required to suppress *de novo* lipogenesis in ITAD-fed mice (Figure 6H). Further, ATG7-depleted livers failed to induce *Pgc1α* and *Fgf21* expression in ITAD-fed mice (Figure 6H), supporting the notion that autophagy coordinates lipohomeostatic responses during ITAD feeding via time-restricted changes in lipophagy and lipogenesis (Figure 4P).

Autophagy in Myf5+ Progenitors Is Required for Glycolytic IIB Fiber Expansion

Because Myf5+ progenitors give rise to muscle, and since ITAD feeding induced *Myf5* expression and autophagy in muscle (Figures 3N and 2G), we explored whether Myf5 progenitor cell-specific autophagy is required for muscle-specific benefits of ITAD feeding. Consistent with immunofluorescence in Figure 3P, GA from 6 month ITAD-fed Con mice displayed an increase in type IIB MyHC protein levels, while TA revealed an increase in embryonic (e)MyHC protein levels without affecting those of MyHC IIA and MyHC I (Figures 6I and 6J). ITAD-fed Con mice also increased their expression of glycolytic genes in GA, *hexokinase 2* (*Hk2*), *phosphofructokinase* (*Pfk*), and *pyruvate kinase* (*Pk*) (Figure S6D). By contrast, ITAD-fed mice lacking *Atg7* in Myf5+ progenitors (*Atg7*KO^{Myf5}) failed to induce *MyHC type IIB* and *eMyHC* protein levels (Figures 6I and 6J) or induce glycolytic gene expression to levels observed in Con (Figure S6D), demonstrating the requirement of autophagy in Myf5+ progenitors for glycolytic type IIB fiber expansion in the context of ITAD feeding. Consistent with these changes, RD-fed *Atg7*KO^{Myf5} mice remained modestly glucose intolerant despite ITAD feeding (Figure 6K). Impaired glucose intolerance in KO mice likely occurred from muscle-intrinsic defects, and not from increased glucose production in liver, since *Atg7*KO^{Myf5} mice displayed reduced basal gluconeogenesis compared with Con in PTT (Figure S6E). In sum, autophagy failure in myogenic progenitors may explain age-associated loss of type IIB fibers that is reversible in part by ITAD feeding.

Autophagy Determines iWAT Mass in ITAD-Fed Mice

Since ITAD feeding reduced fat mass, we next tested whether autophagy is required for the fat-intrinsic benefits of ITAD feeding. Loss of *Atg7* in adipose tissue using the aP2-Cre line revealed eWAT browning and reduced adiposity (Singh et al., 2009b; Zhang et al., 2009); however, aP2 is expressed in several non-adipogenic tissues (Urs et al., 2006). Consequently, we used the adiponectin-Cre line (Eguchi et al., 2011) to delete *Atg7* in WAT to identify the benefits of ITAD feeding that are lost in adipose-specific *Atg7*KO mice (*Atg7*KO^{Adipoq}). Immunoblots revealed loss of ATG7 and accumulation of LC3-I in eWAT and iWAT, validating loss of autophagy (Figure S7A). Loss of *Atg7* did not affect adipocyte differentiation, as indicated by equivalent expression of markers of differentiated fat: *Pparγ*, *aP2*, *C/EBPα*, *C/EBPβ*, *FAS*, and *PLIN1* (Figure S7B). Under basal Ad-lib-fed condition, 5- to 6-month-old RD-fed *Atg7*KO^{Adipoq} mice showed no differences in body wt compared with Con (25.6 ± 0.9 versus 28.3 ± 0.8, p = 0.09, n = 6), and no differences in fat pad wt (data not shown). After 4 months of ITAD feeding on HFD, while ITAD-fed Con mice reduced their body wt by ~20%, ITAD-fed *Atg7*KO^{Adipoq} mice lost only ~7% of their wt (Figure 7A). These data suggest that autophagy is required in adipose tissue (Figure 7A) and POMC neurons (Figure 6A) for the body wt-reducing effect of ITAD feeding. Accordingly, qNMR analyses revealed that *Atg7*KO^{Adipoq} mice failed to significantly lower their body fat content when subjected to 4 months of ITAD feeding (Figure 7B). Intriguingly, while eWAT from ITAD-fed Con and *Atg7*KO^{Adipoq} mice each lost ~50% of their mass (Figure 7C), iWAT from *Atg7*KO^{Adipoq} mice completely resisted losing its mass following ITAD feeding (Figure 7D), demonstrating that autophagy is required for reduction of iWAT mass, but not eWAT mass, in response to ITAD feeding. Since ITAD feeding increases OCR in iWAT (Figure 3G), and not eWAT (Figure 3H), ITAD feeding-driven increase in OCR/EE is likely coupled to loss of iWAT mass.

Autophagy Regulates iWAT Browning and Glucose Homeostasis in ITAD-Fed Mice

Given the effect of ITAD feeding on WAT browning, we investigated the role of autophagy in ITAD feeding-induced iWAT

Figure 5. ITAD Feeding Prevents Age-Associated Metabolic Defects

(A–F) ITAD feeding in young and aged male mice fed HFD for 6 months (A).

Body composition and liver wt normalized to body wt (B and C), liver/serum TG (D and E), and GA-Soleus (Sol) wt normalized to body wt in 10- and 24-month-old male mice (F), as in (A) (n = 3–4).

(G) Young mice fed HFD Ad-lib for 8 months and then ITAD-fed or not for 4 months, and serum TG after 4 months of ITAD feeding (n = 5).

(H–O) VO2, VCO2, EE rates, and z axis movements in young/aged male mice fed Ad-lib on HFD or ITAD-fed on HFD for 6 months (H–K) (n = 3–4). Liver OCR and AUC for OCR (L) (n = 3–4), liver qPCR analyses for mitochondrial and autophagy-related genes (M and N) (n = 8), and net LC3-II flux in liver explants cultured in presence (+) or absence (−) of Lys Inh in aged male mice (O) (n = 8).

(P and Q) Glucose tolerance tests (GTTs) and AUC in HFD-fed aged and young male mice on Ad-lib or ITAD feeding for 6 months (n = 6).

Bars are mean ± SEM. *p < 0.05, **p < 0.01, ***p < 0.001. Student's t test. See also Figure S4.

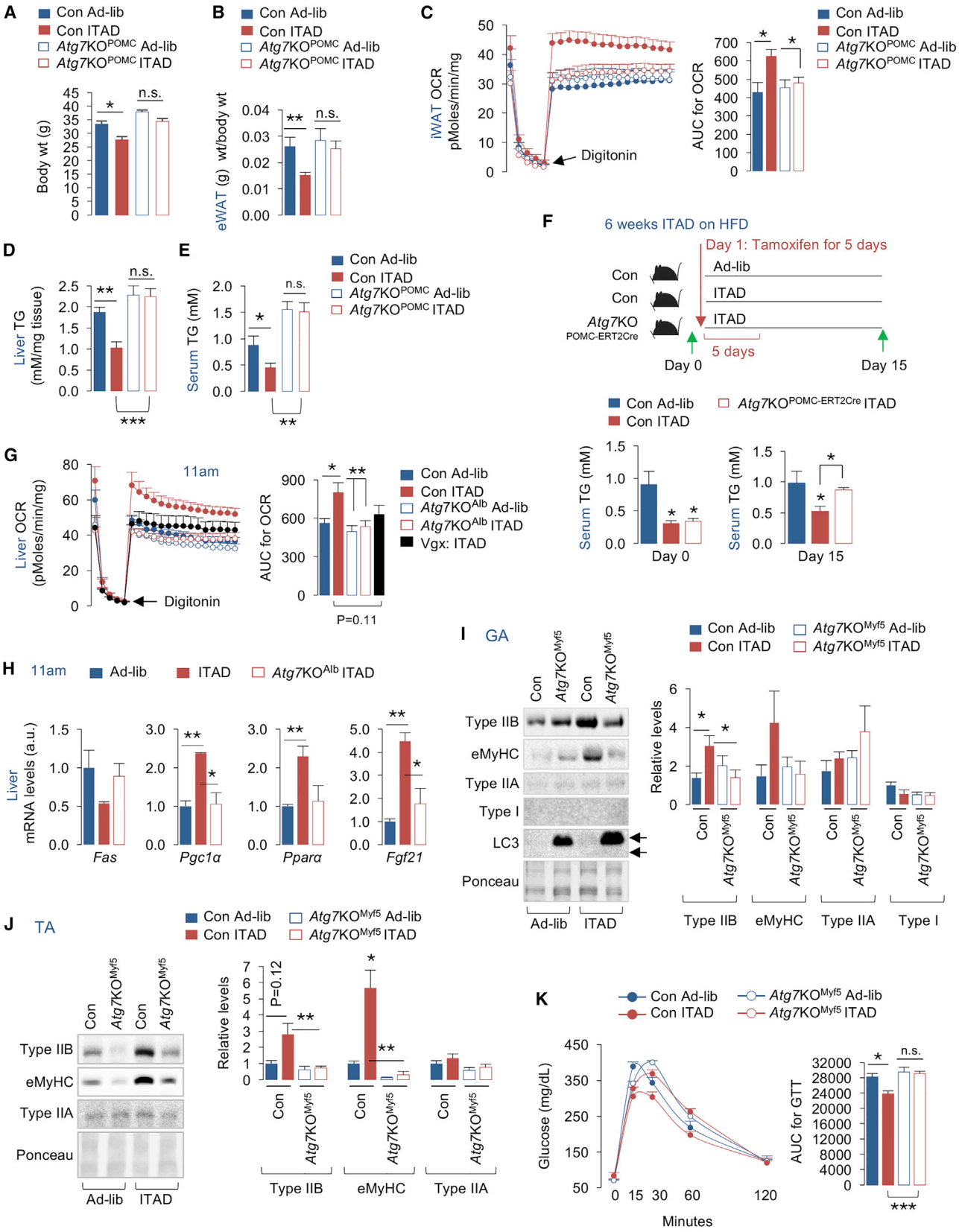

(legend on next page)

browning. Our studies revealed that ITAD feeding led to induction of UCP1 (Figure 3C), and *Eva1*, *Zic1*, and *Fbxo31* in iWAT, indicating adipose browning (Figure 3D). Notably, loss of *Atg7* blocked ITAD-driven WAT browning, as indicated by reduced expression of *Eva1* and *Zic1* (Figures 7E and 7F). Consistent with these changes, *Atg7*KO^{Adipoq} mice failed to decrease their adipocyte size (Figure S7C) or increase their VO2, VCO2, and EE rates in response to ITAD feeding (Figures 7G–7I). Failure to increase their EE was not due to reduced locomotion since all groups displayed equivalent activity (Figure 7J). Although ITAD feeding reduced eWAT mass (Figure 7C) and lowered serum leptin levels to varying degrees in Con and *Atg7*KO^{Adipoq} mice (Figure 7K, left), ITAD-fed KO mice remained modestly glucose intolerant (Figure S7D) and insulin insensitive, as indicated by elevated serum insulin levels (Figure 7K, right) compared with Con. Most surprisingly, impaired glucose clearance in ITAD-fed *Atg7*KO^{Adipoq} mice occurred in part from failure to suppress gluconeogenesis when subjected to PTT (Figure 7L) suggesting that adipose autophagy contributes to ITAD feeding-driven lipid/glucose homeostasis by modulating iWAT browning and hepatic glucose production.

DISCUSSION

Here we show that ITAD feeding/intermeal fasting in absence of CR promotes metabolic flexibility and prevents age/obesity-associated metabolic defects. Consolidating the system-wide metabolic benefits of ITAD feeding (Figure 7M), we have found that ITAD feeding/intermeal fasting activates autophagy in liver, adipose tissue, muscle, and MBH at 11 a.m. LC3-II flux analyses in liver at each of the six time points revealed that autophagy is modified in a time-dependent manner in ITAD-fed mice. This time-restricted change in autophagy is characterized by: (1) maximal activation at 11 a.m. in response to feeding between 8 and 10 a.m. and its suppression at 7 p.m. immediately after the second feeding window, and (2) a complete shift in phase of LC3-II flux compared with Con. Induction of autophagy at 11 a.m. led to expression of key drivers of fat utilization, *Ppar*α, *Fgf21*, and *Pgc1*α, since acutely depleting *Atg7* in liver blocked ITAD feeding-driven expression of these genes. Since PPARα signaling induces autophagy (Lee et al., 2014), it is possible that feedforward autophagy-PPARα-lipophagy regulatory loops help maximize fat utilization during ITAD feeding. Interestingly, although autophagy flux decreased at 7 p.m. in ITAD mice, KO of *Atg7* via *Cre* injections reversed the suppression of lipogenesis between 3 and 11 p.m., indicating a role of autophagy in suppression of lipogenesis in ITAD-fed mice. However, how autophagy activity is modified in ITAD-fed mice, and how this impacts *de novo* lipogenesis, is unknown and will remain the subject of future studies. Our data allow us to speculate that AMPK and mTOR and their opposing influences on autophagy activator protein ULK1/ATG1 could potentially reorganize autophagy in response to changes in nutrient availability; however, validation of this notion will require future studies. In sum, activation of autophagy and increased fat utilization during the first feeding window, and suppression of lipogenesis at 7 p.m., act in concert to decrease liver TG in ITAD-fed mice (Figure 4P). In accordance with findings that cold-induced lipophagy in liver is governed by functional autophagy in POMC neurons (Martinez-Lopez et al., 2016), we propose that POMCergic autophagy is required for ITAD feeding-driven fat utilization in liver and iWAT, solidifying the integrative physiology of CNS to peripheral autophagy in energy balance.

ITAD feeding led to significant brown fat-like remodeling of iWAT and an abundance of markers of anti-inflammatory M2 macrophage in eWAT. Brown fat-like remodeling of iWAT was autophagy dependent, since iWAT from *Atg7*KO^{Adipoq} mice displayed reduced browning and decreased EE rates. However, we were most surprised to find that, while ITAD feeding reduced eWAT mass in both Con and *Atg7*KO^{Adipoq}, *Atg7*KO^{Adipoq} mice failed to decrease their iWAT mass in response to ITAD feeding. While we are unable to explain these results, it is possible that different origins or innervation patterns of distinct fat depots is the reason why autophagy is required in iWAT, and not eWAT, for the benefits of ITAD feeding.

A major benefit of ITAD feeding is improved glucose tolerance. ITAD-fed *Atg7*KO^{POMC} and Con mice each displayed similar improvements in glucose clearance, which excluded the requirement of POMCergic autophagy for glucose homeostasis in the context of ITAD feeding. By contrast, ITAD-fed *Atg7*KO^{Adipoq} and *Atg7*KO^{Myf5} mice each failed to completely improve glucose clearance rates, indicating that autophagy is required in these tissue systems for ITAD feeding-driven control of glucose homeostasis (Figure 7M). Since improved glucose clearance in ITAD mice was associated with increased glycolytic type IIB fiber number and increased expression of glycolytic genes in GA, it is possible that ITAD feeding enhances the efficiency of skeletal muscles to take up glucose in an autophagy-dependent manner. Supporting this contention, ITAD-fed *Atg7*KO^{Myf5} mice failed to increase their glycolytic type IIB fibers or increase expression of glycolytic genes compared with Con. ITAD feeding suppressed gluconeogenesis to similar levels in *Atg7*KO^{Myf5} and Con mice, excluding the role of hepatic gluconeogenesis in

Figure 6. Tissue-Specific Autophagy Contributes to Distinct Benefits of ITAD Feeding

(A) Body wt of HFD-fed Ad-lib and ITAD-fed Con and *Atg7*KO^{POMC} male mice for 4 months (n = 5).

(B–E) eWAT wt normalized to body wt in males (B) (n = 6), iWAT OCR and AUC for OCR in male (n = 3) and female (n = 3) mice (C) (total n = 6), liver TG in males (n = 7) and females (n = 5) (D) (total n = 12), and serum TG in HFD-fed Con and *Atg7*KO^{POMC} male (n = 3) and female mice (n = 3) fed Ad-lib or ITAD for 4 months (E) (total n = 6).

(F) Serum TG on day 0 and day 15 (as indicated) in control and *Atg7*KO$^{POMC-ERT2-Cre}$ male mice fed Ad-lib or ITAD on HFD for 6 weeks and subjected to tamoxifen injections for 5 days (n = 6).

(G) Liver OCR and AUC from Con and *Atg7*KO^{Alb} mice fed Ad-lib or ITAD on RD for 6 months, and in male mice subjected to vagotomy (Vgx) and ITAD feeding on RD for 6 months (n = 3–5).

(H) Liver qPCR analyses for indicated genes from RD-fed Ad-lib, and ITAD-fed Con and *Atg7*KO^{Alb} male mice for 6 months (n = 3).

(I–K) IB for indicated proteins in GA (I), TA (J), and GTT (K) in RD-fed Con and *Atg7*KO^{Myf5} male (n = 3) and female mice (n = 3) fed Ad-lib and ITAD for 6 months (total n = 6). Ponceau is loading control.

Bars are mean ± SEM. *p < 0.05, **p < 0.01, ***p < 0.001, n.s., not significant. Student's t test or two-factor ANOVA and Bonferroni correction. See also Figure S6.

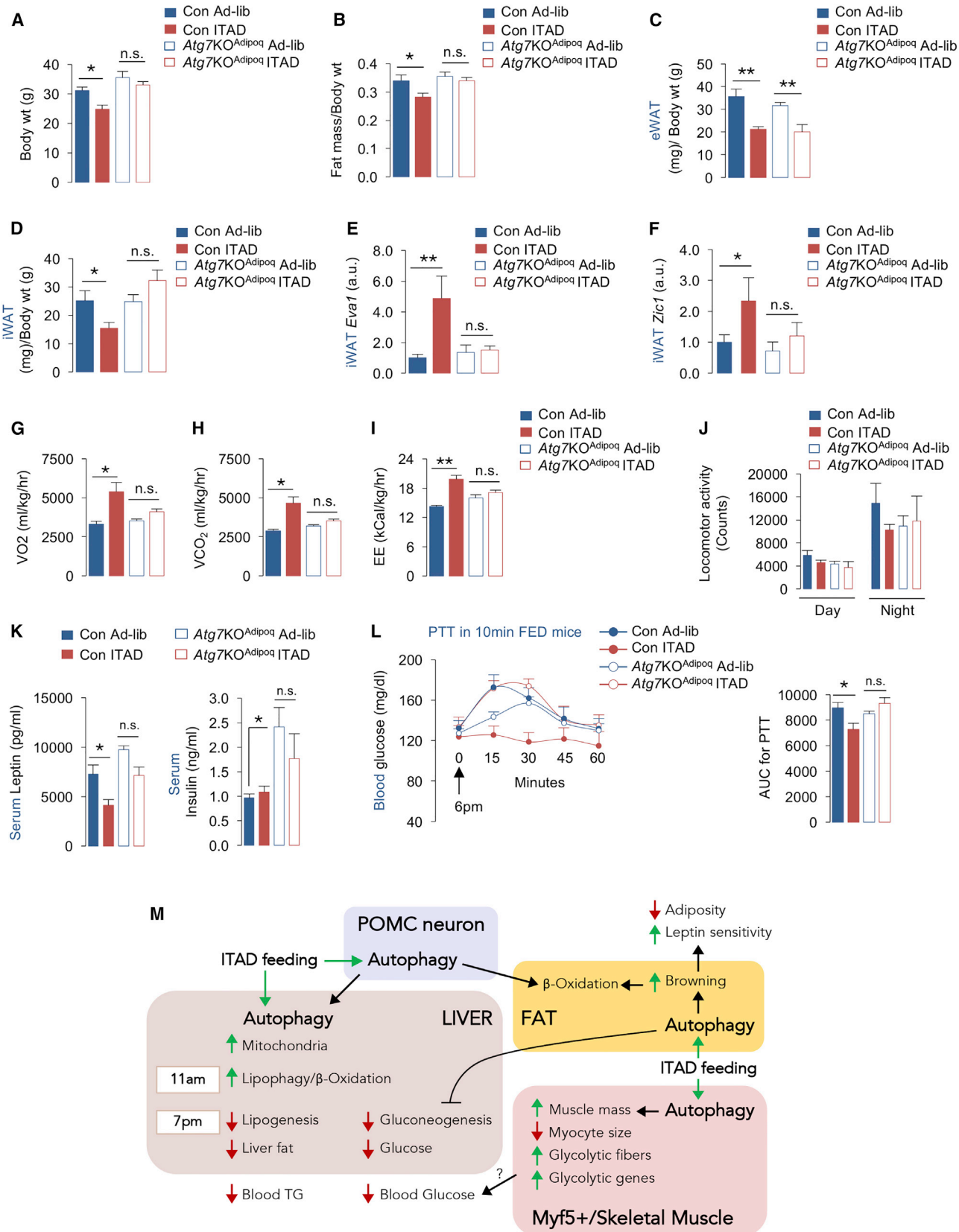

(legend on next page)

altered glucose homeostasis in *Atg7*KO^{Myf5} mice. Surprisingly, ITAD-fed *Atg7*KO^{Adipoq} mice remained pyruvate intolerant, indicating that adipose autophagy is required to suppress hepatic gluconeogenesis in ITAD-fed mice, although the inter-organ crosstalk linking adipose autophagy to hepatic gluconeogenesis remains unknown.

In sum, CR robustly extends healthspan; however, CR is associated with muscle loss, and there may be circumstances when CR is counterproductive, such as during advanced aging or sarcopenia. Furthermore, twice-a-day feeding has been shown to improve glycemia in human diabetics compared with those fed six meals a day (Kahleova et al., 2014). Based on our diurnal feeding strategy in nocturnally active mice, we do not imply that humans should have two meals at night; rather, our results suggest that distributing calories into two meals per circadian period could prevent metabolic defects. In addition, comparisons between twice-a-day feeding with three or more feeding intervals per day were not performed in this study, and future studies are necessary to determine the impact of the various meal partitioning strategies on healthspan outcome. We present a compliable feeding strategy that through time-dependent induction of autophagy may prevent age/obesity-induced metabolic decline without the need for CR or changing the type of food consumed.

STAR★METHODS

Detailed methods are provided in the online version of this paper and include the following:

- KEY RESOURCES TABLE
- CONTACT FOR REAGENT AND RESOURCE SHARING
- EXPERIMENTAL MODEL AND SUBJECT DETAILS
  - Animals
  - Housing
  - Isocaloric Twice-a-Day Feeding (ITAD)/Intermeal Fasting
- METHOD DETAILS
  - Autophagy Flux Assay
  - RNA Isolation and qPCR Analyses
  - Histological Analyses
  - Immunohistochemistry
  - Metabolic Profiling
  - Tissue Respirometry
  - Vagotomy
  - Adenoviral Cre Expression
  - Stromal Vascular Fraction Isolation
  - Glucose Tolerance Test (GTT)
  - Pyruvate Tolerance Test (PTT)
  - Biochemical Analyses
  - Western Blotting
- QUANTIFICATION AND STATISTICAL ANALYSIS

SUPPLEMENTAL INFORMATION

Supplemental Information includes seven figures and one table and can be found with this article online at https://doi.org/10.1016/j.cmet.2017.09.020.

AUTHOR CONTRIBUTIONS

N.M.-L. and E.T. performed the experiments and analyzed data. S.S., M.T., M.G.-M., and A.B.-G. assisted with *in vivo* experiments. G.J.S., N.B., J.E.P., and S.K. provided intellectual input. R.S. conceived the idea, designed the experiments, interpreted data, and wrote the manuscript. All authors commented on the manuscript.

ACKNOWLEDGMENTS

We thank Drs. M. Komatsu and K. Tanaka (Tokyo Metropolitan Institute of Medical Science, Japan) for *Atg7*$^{flox/flox}$ mice, Dr. J. Elmquist (UT Southwestern Medical Center, USA) for POMC-ERT2-Cre mice, and Dr. F. Villarroya (University of Barcelona) for helpful suggestions. This work was supported by R01 AG043517 (to R.S.), P30 DK020541 (Einstein Diabetes Research Center), and P01 AG031782 (to R.S.). A.B.-G. is supported by NIH NIA T32 AG023475. M.T. is supported by American Diabetes Association grant 1-17-PMF-011. I thank N.M.-L., E.T., S.S., M.T., A.B.-G., and M.G.-M, who participated in ITAD feeding of our colonies twice each day for the last 6 years come rain or snow.

Received: November 23, 2016
Revised: June 28, 2017
Accepted: September 25, 2017
Published: October 26, 2017

REFERENCES

Anson, R.M., Guo, Z., de Cabo, R., Iyun, T., Rios, M., Hagepanos, A., Ingram, D.K., Lane, M.A., and Mattson, M.P. (2003). Intermittent fasting dissociates beneficial effects of dietary restriction on glucose metabolism and neuronal resistance to injury from calorie intake. Proc. Natl. Acad. Sci. USA *100*, 6216–6220.

Badman, M.K., Pissios, P., Kennedy, A.R., Koukos, G., Flier, J.S., and Maratos-Flier, E. (2007). Hepatic fibroblast growth factor 21 is regulated by PPARalpha and is a key mediator of hepatic lipid metabolism in ketotic states. Cell Metab. *5*, 426–437.

Bass, J., and Takahashi, J.S. (2010). Circadian integration of metabolism and energetics. Science *330*, 1349–1354.

Berglund, E.D., Liu, C., Sohn, J.W., Liu, T., Kim, M.H., Lee, C.E., Vianna, C.R., Williams, K.W., Xu, Y., and Elmquist, J.K. (2013). Serotonin 2C receptors in pro-opiomelanocortin neurons regulate energy and glucose homeostasis. J. Clin. Invest. *123*, 5061–5070.

Berry, R., and Rodeheffer, M.S. (2013). Characterization of the adipocyte cellular lineage in vivo. Nat. Cell Biol. *15*, 302–308.

Figure 7. Autophagy Is Required for iWAT Browning in ITAD-Fed Mice

(A–D) Body wt (A) and fat mass , eWAT wt, and iWAT wt normalized to body wt in Con and *Atg7*KO^{Adipoq} male (n = 3) and female mice (n = 3) subjected to Ad-lib or ITAD feeding on HFD for 4 months (B–D) (total n = 6).

(E and F) qPCR for Beige genes *Eva1* and *Zic1* in iWAT from Con and *Atg7*KO^{Adipoq} male and female mice subjected to Ad-lib or ITAD feeding on HFD for 4 months (n = 6).

(G–J) VO2, VCO2, EE rates, and locomotor activity in Con and *Atg7*KO^{Adipoq} male and female mice subjected to Ad-lib or ITAD feeding on HFD for 4 months (n = 6).

(K) Serum leptin and insulin levels in Con and *Atg7*KO^{Adipoq} male and female mice subjected to Ad-lib or ITAD feeding on HFD for 4 months (n = 6).

(L) PTT and AUC for PTT at 6 p.m. in Ad-lib and ITAD-fed Con and *Atg7*KO^{Adipoq} male and female mice fed for 10 min at 5 p.m. (n = 6).

(M) Proposed model for contribution of tissue-specific autophagy to metabolic benefits of ITAD feeding.

Bars are mean ± SEM. *p < 0.05, **p < 0.01, n.s., not significant. Two-factor ANOVA and Bonferroni correction. See also Figure S7.

Bouhlel, M.A., Derudas, B., Rigamonti, E., Dievart, R., Brozek, J., Haulon, S., Zawadzki, C., Jude, B., Torpier, G., Marx, N., et al. (2007). PPARgamma activation primes human monocytes into alternative M2 macrophages with anti-inflammatory properties. Cell Metab. *6*, 137–143.

Brandhorst, S., Choi, I.Y., Wei, M., Cheng, C.W., Sedrakyan, S., Navarrete, G., Dubeau, L., Yap, L.P., Park, R., Vinciguerra, M., et al. (2015). A periodic diet that mimics fasting promotes multi-system regeneration, enhanced cognitive performance, and healthspan. Cell Metab. *22*, 86–99.

Chaix, A., Zarrinpar, A., Miu, P., and Panda, S. (2014). Time-restricted feeding is a preventative and therapeutic intervention against diverse nutritional challenges. Cell Metab. *20*, 991–1005.

Charge, S.B., and Rudnicki, M.A. (2004). Cellular and molecular regulation of muscle regeneration. Physiol. Rev. *84*, 209–238.

Colman, R.J., Anderson, R.M., Johnson, S.C., Kastman, E.K., Kosmatka, K.J., Beasley, T.M., Allison, D.B., Cruzen, C., Simmons, H.A., Kemnitz, J.W., et al. (2009). Caloric restriction delays disease onset and mortality in rhesus monkeys. Science *325*, 201–204.

Coupe, B., Ishii, Y., Dietrich, M.O., Komatsu, M., Horvath, T.L., and Bouret, S.G. (2012). Loss of autophagy in pro-opiomelanocortin neurons perturbs axon growth and causes metabolic dysregulation. Cell Metab. *15*, 247–255.

Dalle Pezze, P., Ruf, S., Sonntag, A.G., Langelaar-Makkinje, M., Hall, P., Heberle, A.M., Razquin Navas, P., van Eunen, K., Tolle, R.C., Schwarz, J.J., et al. (2016). A systems study reveals concurrent activation of AMPK and mTOR by amino acids. Nat. Commun. *7*, 13254.

Damiola, F., Le Minh, N., Preitner, N., Kornmann, B., Fleury-Olela, F., and Schibler, U. (2000). Restricted feeding uncouples circadian oscillators in peripheral tissues from the central pacemaker in the suprachiasmatic nucleus. Genes Dev. *14*, 2950–2961.

Egan, D.F., Shackelford, D.B., Mihaylova, M.M., Gelino, S., Kohnz, R.A., Mair, W., Vasquez, D.S., Joshi, A., Gwinn, D.M., Taylor, R., et al. (2011). Phosphorylation of ULK1 (hATG1) by AMP-activated protein kinase connects energy sensing to mitophagy. Science *331*, 456–461.

Eguchi, J., Wang, X., Yu, S., Kershaw, E.E., Chiu, P.C., Dushay, J., Estall, J.L., Klein, U., Maratos-Flier, E., and Rosen, E.D. (2011). Transcriptional control of adipose lipid handling by IRF4. Cell Metab. *13*, 249–259.

He, C., Bassik, M.C., Moresi, V., Sun, K., Wei, Y., Zou, Z., An, Z., Loh, J., Fisher, J., Sun, Q., et al. (2012). Exercise-induced BCL2-regulated autophagy is required for muscle glucose homeostasis. Nature *481*, 511–515.

Heilbronn, L.K., Smith, S.R., Martin, C.K., Anton, S.D., and Ravussin, E. (2005). Alternate-day fasting in nonobese subjects: effects on body weight, body composition, and energy metabolism. Am. J. Clin. Nutr. *81*, 69–73.

Inagaki, T., Dutchak, P., Zhao, G., Ding, X., Gautron, L., Parameswara, V., Li, Y., Goetz, R., Mohammadi, M., Esser, V., et al. (2007). Endocrine regulation of the fasting response by PPARalpha-mediated induction of fibroblast growth factor 21. Cell Metab. *5*, 415–425.

Iqbal, J., Li, X., Chang, B.H., Chan, L., Schwartz, G.J., Chua, S.C., Jr., and Hussain, M.M. (2010). An intrinsic gut leptin-melanocortin pathway modulates intestinal microsomal triglyceride transfer protein and lipid absorption. J. Lipid Res. *51*, 1929–1942.

Kahleova, H., Belinova, L., Malinska, H., Oliyarnyk, O., Trnovska, J., Skop, V., Kazdova, L., Dezortova, M., Hajek, M., Tura, A., et al. (2014). Eating two larger meals a day (breakfast and lunch) is more effective than six smaller meals in a reduced-energy regimen for patients with type 2 diabetes: a randomised crossover study. Diabetologia *57*, 1552–1560.

Karsli-Uzunbas, G., Guo, J.Y., Price, S., Teng, X., Laddha, S.V., Khor, S., Kalaany, N.Y., Jacks, T., Chan, C.S., Rabinowitz, J.D., et al. (2014). Autophagy is required for glucose homeostasis and lung tumor maintenance. Cancer Discov. *4*, 914–927.

Kaushik, S., Arias, E., Kwon, H., Lopez, N.M., Athonvarangkul, D., Sahu, S., Schwartz, G.J., Pessin, J.E., and Singh, R. (2012). Loss of autophagy in hypothalamic POMC neurons impairs lipolysis. EMBO Rep. *13*, 258–265.

Komatsu, M., Waguri, S., Chiba, T., Murata, S., Iwata, J., Tanida, I., Ueno, T., Koike, M., Uchiyama, Y., Kominami, E., et al. (2006). Loss of autophagy in the central nervous system causes neurodegeneration in mice. Nature *441*, 880–884.

Lamia, K.A., Sachdeva, U.M., DiTacchio, L., Williams, E.C., Alvarez, J.G., Egan, D.F., Vasquez, D.S., Juguilon, H., Panda, S., Shaw, R.J., et al. (2009). AMPK regulates the circadian clock by cryptochrome phosphorylation and degradation. Science *326*, 437–440.

Lee, J.M., Wagner, M., Xiao, R., Kim, K.H., Feng, D., Lazar, M.A., and Moore, D.D. (2014). Nutrient-sensing nuclear receptors coordinate autophagy. Nature *516*, 112–115.

Martinez-Lopez, N., Athonvarangkul, D., Sahu, S., Coletto, L., Zong, H., Bastie, C.C., Pessin, J.E., Schwartz, G.J., and Singh, R. (2013). Autophagy in Myf5+ progenitors regulates energy and glucose homeostasis through control of brown fat and skeletal muscle development. EMBO Rep. *14*, 795–803.

Martinez-Lopez, N., Garcia-Macia, M., Sahu, S., Athonvarangkul, D., Liebling, E., Merlo, P., Cecconi, F., Schwartz, G.J., and Singh, R. (2016). Autophagy in the CNS and periphery coordinate lipophagy and lipolysis in the brown adipose tissue and liver. Cell Metab. *23*, 113–127.

Marzetti, E., Lees, H.A., Wohlgemuth, S.E., and Leeuwenburgh, C. (2009). Sarcopenia of aging: underlying cellular mechanisms and protection by calorie restriction. Biofactors *35*, 28–35.

Masiero, E., Agatea, L., Mammucari, C., Blaauw, B., Loro, E., Komatsu, M., Metzger, D., Reggiani, C., Schiaffino, S., and Sandri, M. (2009). Autophagy is required to maintain muscle mass. Cell Metab. *10*, 507–515.

Mattison, J.A., Roth, G.S., Beasley, T.M., Tilmont, E.M., Handy, A.M., Herbert, R.L., Longo, D.L., Allison, D.B., Young, J.E., Bryant, M., et al. (2012). Impact of caloric restriction on health and survival in rhesus monkeys from the NIA study. Nature *489*, 318–321.

Moreira, E.A., Most, M., Howard, J., and Ravussin, E. (2011). Dietary adherence to long-term controlled feeding in a calorie-restriction study in overweight men and women. Nutr. Clin. Pract. *26*, 309–315.

Narita, M., Young, A.R., Arakawa, S., Samarajiwa, S.A., Nakashima, T., Yoshida, S., Hong, S., Berry, L.S., Reichelt, S., Ferreira, M., et al. (2011). Spatial coupling of mTOR and autophagy augments secretory phenotypes. Science *332*, 966–970.

Quan, W., Kim, H.K., Moon, E.Y., Kim, S.S., Choi, C.S., Komatsu, M., Jeong, Y.T., Lee, M.K., Kim, K.W., Kim, M.S., et al. (2012). Role of hypothalamic proopiomelanocortin neuron autophagy in the control of appetite and leptin response. Endocrinology *153*, 1817–1826.

Rajakumari, S., Wu, J., Ishibashi, J., Lim, H.W., Giang, A.H., Won, K.J., Reed, R.R., and Seale, P. (2013). EBF2 determines and maintains brown adipocyte identity. Cell Metab. *17*, 562–574.

Rubinsztein, D.C., Marino, G., and Kroemer, G. (2011). Autophagy and aging. Cell *146*, 682–695.

Singh, R., Kaushik, S., Wang, Y., Xiang, Y., Novak, I., Komatsu, M., Tanaka, K., Cuervo, A.M., and Czaja, M.J. (2009a). Autophagy regulates lipid metabolism. Nature *458*, 1131–1135.

Singh, R., Xiang, Y., Wang, Y., Baikati, K., Cuervo, A.M., Luu, Y.K., Tang, Y., Pessin, J.E., Schwartz, G.J., and Czaja, M.J. (2009b). Autophagy regulates adipose mass and differentiation in mice. J. Clin. Invest. *119*, 3329–3339.

Urs, S., Harrington, A., Liaw, L., and Small, D. (2006). Selective expression of an aP2/fatty acid binding protein 4-Cre transgene in non-adipogenic tissues during embryonic development. Transgenic Res. *15*, 647–653.

Varady, K.A., Bhutani, S., Church, E.C., and Klempel, M.C. (2009). Short-term modified alternate-day fasting: a novel dietary strategy for weight loss and cardioprotection in obese adults. Am. J. Clin. Nutr. *90*, 1138–1143.

Wu, J., Bostrom, P., Sparks, L.M., Ye, L., Choi, J.H., Giang, A.H., Khandekar, M., Virtanen, K.A., Nuutila, P., Schaart, G., et al. (2012). Beige adipocytes are a distinct type of thermogenic fat cell in mouse and human. Cell *150*, 366–376.

Zhang, Y., Goldman, S., Baerga, R., Zhao, Y., Komatsu, M., and Jin, S. (2009). Adipose-specific deletion of autophagy-related gene 7 (atg7) in mice reveals a role in adipogenesis. Proc. Natl. Acad. Sci. USA *106*, 19860–19865.

STAR★METHODS

KEY RESOURCES TABLE

REAGENT or RESOURCE	SOURCE	IDENTIFIER
Antibodies		
Rabbit polyclonal anti-ATG7	Cell Signaling Technology	CS2631; RRID: AB_2227783
Rabbit polyclonal anti-LC3B	Cell Signaling Technology	CS2775; RRID: AB_915950
Rabbit polyclonal anti-ATG12-ATG5	Novus Biologicals	NB110-53818; RRID: AB_828587
Mouse monoclonal anti-Beclin1	BD Biosciences	612112; RRID: AB_399483
Mouse monoclonal anti-Myosin heavy chain (MyHC) Type IIB fiber	Developmental Studies Hybridoma Bank	BF-F3; RRID: AB_2266724
Mouse monoclonal anti-Embryonic Myosin heavy chain (eMyHC) fiber	Developmental Studies Hybridoma Bank	BF-G6; RRID: AB_10571455
Mouse monoclonal anti-Myosin heavy chain (MyHC) Type IIA fiber	Developmental Studies Hybridoma Bank	SC-71; RRID: AB_2147165
Mouse monoclonal anti-Myosin heavy chain (MyHC) Type I fiber	Developmental Studies Hybridoma Bank	BA-D5; RRID: AB_2235587
Rabbit polyclonal anti-p62	Enzo Life Technology	BML-PW9860; RRID: AB_2196009
Rabbit polyclonal anti-F4/80	Invitrogen	PA5-32399; RRID: AB_2549869
Rabbit polyclonal anti-β-actin	Abcam	ab8227; RRID: AB_2305186
Mouse monoclonal anti-GAPDH	Abcam	ab8245; RRID: AB_2107448
Rabbit polyclonal anti-UCP1	Abcam	ab10983; RRID: AB_2241462
Secondary HRP Antibody Rabbit anti-Mouse IgG	Invitrogen	61-6520; RRID: AB_2533933
Secondary HRP Antibody Goat anti-Rabbit IgG	KPL	074-1506
Secondary Antibody Donkey anti-Mouse Alexa-Fluo488	Invitrogen	A21202; RRID: AB_141607
Bacterial and Virus Strains		
Control Adenovirus	Vector Biolabs	1060
Cre-expressing Adenovirus	Vector Biolabs	1700
Chemicals, Peptides, and Recombinant Proteins		
High Fat Diet (HFD- 60% of calories in fat)	Research Diet	D12492
PicoLab Rodent Diet	Lab Diet	5058
Isoflurane	Henry Schein	029405
Leupeptin hemisulfate	Fisher Scientific	BP2662100
Ammonium Chloride	American Bioanalytical	AB00161
Trizol Reagent	Invitrogen	15596018
Superscript II Reverse Transcriptase	Invitrogen	18064014
Hematoxylin	Poly-scientific	S212
Eosin	StatLab	SL98-1
Digitonin	Sigma-Aldrich	D5628
Carnitine	Sigma-Aldrich	C0283
ATP	Sigma-Aldrich	A2383
NAD	Sigma-Aldrich	N0632
Co-enzyme A	Sigma-Aldrich	C3144
Sodium Pyruvate	Sigma-Aldrich	P2256
D-Glucose	Fisher Scientific	D16-500
SODIUM PHOSPHATE, DIBASIC, ANHYDROUS	American Bioanalytical	AB02050
Sodium Chloride	American Bioanalytical	AB01915
Collagenase Type I	Worthington Biochemical Corporation	LS004196

(*Continued on next page*)

Continued

REAGENT or RESOURCE	SOURCE	IDENTIFIER
Penicillin/Streptomycin	Invitrogen	15070063
DMEM high glucose	Invitrogen	11965118
Fetal Calf Serum	Invitrogen	12103C
Power SYBR Green PCR Master Mix	Invitrogen	4368708
RNeasy Plus Mini kit	Qiagen	74136
Pepsin	BioCare Medical	PEP959H
Trypsin	Gibco	15090
Bovine Serum Albumin	American Bioanalytical	AB00440
Donkey Serum	Sigma-Aldrich	S30
Super Picture DAB Kit	Invitrogen	879263
VECTASTAIN Elite ABC HRP Kit	Vector	PK-6100
Triton X-100	Sigma-Aldrich	X100-500ml
30% Acrylamide/ Bis Solution 37-5-1	BioRad	161-0158
Sodium Pyrophosphate	Sigma-Aldrich	AB02014
Pepstatin A	Sigma-Aldrich	P4265
β-Glycerophosphate	Sigma-Aldrich	G9891
Sodium Orthovanadate	Sigma-Aldrich	S6508
PMSF	Sigma-Aldrich	10837091001
AEBSF	Fisher Scientific	BP2644500
Ethylenediaminetetraacetic acid (EDTA)	American Bioanalytical	AB00500
Ethylene glycol-bis(2-aminoethyl)-tetraacetic acid (EGTA)	American Bioanalytical	AB00505
Super Signal West Femto Maximum Sensitivity Substrate, ECL	Pierce	34096
Critical Commercial Assays		
ELISA Insulin Kit	ALPCO	80-INSHU-E01.1
ELISA FGF21 mouse/rat	R&D System	MF2100
ELISA Leptin Kit	SPI Bio	A05176
TG assay kit	Sigma-Aldrich	TR0100
Experimental Models: Organisms/Strains		
Mouse: C57BL/6 wildtype	The Jackson Laboratory	JAX: 000664
Mouse POMC-Cre: (*B6.FVB-Tg(Pomc-cre)1Lowl/J*	The Jackson Laboratory	JAX: 010714
Mouse POMC-ERT2-Cre	Berglund et al., (2013)	N/A
Mouse Myf5-Cre: *B6.129S4-Myf5$^{tm3(cre)Sor}$/J*	The Jackson Laboratory	JAX: 007893
Mouse Adiponectin-Cre: *B6;FVB-Tg(Adipoq-cre)1Evdr/J*	The Jackson Laboratory	JAX: 010803
Mouse Atg7$^{flox/flox}$	Komatsu et al., (2006)	N/A
Mouse: C57BL/6 Young/Old	NIH NIA	N/A
Oligonucleotides		
RT-PCR primers Please see Table S1	Sigma-Aldrich	N/A
Software and Algorithms		
ImageJ	NIH	https://imagej.nih.gov/ij/index.html; RRID: SCR_003070
Prism	Graph Pad	https://www.graphpad.com/scientificsoftware/prism/; RRID: SCR_002798
Other		
Nikon Light Microscope	Nikon	N/A
Axiovert 200 Fluorescence microscope	Carl Zeiss	N/A

(*Continued on next page*)

Continued

REAGENT or RESOURCE	SOURCE	IDENTIFIER
Seahorse Bioscience XF24-3 Extracellular Flux Analyzer	Seahorse Bioscience (Agilent technologies)	N/A
XF24-3 Flux Pak	Seahorse Bioscience (Agilent technologies)	102070-001
XF24 Islet Capture Microplates	Seahorse Bioscience (Agilent technologies)	101122-100
StepOne Plus Real-Time PCR System	Thermo Fisher Scientific	4376600
Cryostat	Leica Biosystems	CM3050S
ECHO magnetic resonance spectroscopy	Echo Medical Systems	N/A
CLAMS open-circuit indirect calorimetry	Columbus Instruments	N/A
Ascensia Contour Glucometer	Bayer	7151H
Ascensia Contour strips	Bayer	7080G
Chemoluminescence Imaging System	Syngene	GeneGnome 5
Cautery Unit	Geiger Medical	N/A

CONTACT FOR REAGENT AND RESOURCE SHARING

Further information and requests for resources and reagents should be directed to the Lead Contact, Rajat Singh (rajat.singh@einstein.yu.edu).

EXPERIMENTAL MODEL AND SUBJECT DETAILS

Animals

Tissue-specific *Atg7* KO mice were generated by crossing *Atg7*$^{flox/flox}$ mice (Komatsu et al., 2006) (Drs. M. Komatsu and K. Tanaka, Tokyo Metropolitan Institute of Medical Science, Japan) with POMC-Cre mice (*B6.FVB-Tg(Pomc-cre)1Lowl/J*; Stock No: 010714; The Jackson Laboratory, Bar Harbor, ME, USA), Myf5-Cre (*B6.129S4-Myf5tm3(cre)Sor/J*; Stock No: 007893; The Jackson Laboratory), Adiponectin-Cre (*B6;FVB-Tg(Adipoq-cre)1Evdr/J*; stock number 010803; The Jackson Laboratory) or POMC-ERT2-Cre mouse (Berglund et al., 2013) (Dr. Joel Elmquist, UT Southwestern Medical Center, Dallas, USA) respectively. Studies were performed in male and female littermates on the C57BL/6J background using a protocol approved by the Institutional Animal Care and Use Committee. All experiments were carried out in group-housed mice. Mice aged between 3mo and 24mo were utilized for the studies. Since no sex-specific differences were observed with regard to the benefits of ITAD feeding on body weight and body fat content, male and female mice were pooled together in a subset of experiments. The distribution of male and female mice in each of these experiments is indicated in the Figure legends. Due to the longitudinal nature of the studies in diverse tissue-specific knockout mice, in-depth analyses of the sex-specific differences on the effects of ITAD feeding were not carried out. Tissues were collected at specific time-points as indicated in Figure legends. The duration of ITAD feeding for each experiment are indicated in Figure legends. Mice were fed a regular chow (5058; Lab Diet, St Louis, MO, USA) or high fat diet (60% kcal in fat; D12492; Research Diets, New Brunswick, NJ, USA). The following inclusion/exclusion criteria were used for the studies. Rodents were excluded and euthanized: (i) if core body temperature dropped below 25°C during the cold exposure studies, and (ii) if they failed to return to normal activity within 12 hr of surgery. Conventional genotyping was carried out to exclude mice heterozygous for *Atg7* deficiency.

Housing

Mice were maintained at 22-23°C on 12 hr light/dark cycles in the institutional barrier facility along with sentinel cages and are specific pathogen-free. Mice in sentinel cages are routinely tested for specific pathogens, and health reports are evaluated at regular intervals to determine whether rodents are pathogen-free or whether a specific treatment is required.

Isocaloric Twice-a-Day Feeding (ITAD)/Intermeal Fasting

ITAD mice were fed the same amount of food as ad libitum (Ad-lib) mice but only in two 2 hr windows each day (8–10am and 5–7pm). The amount of food consumed in the two 2 hr windows by ITAD mice was identical to the food consumed by the Ad-lib group in the preceding 24 hr. Both cohorts were group housed. The ITAD test group and its Ad-lib control (Con) contained the same number of age and sex-matched littermate male or female mice. Food pellets were weighed each day in the barrier facility and broken into smaller pieces and distributed across each cage. Residual food pellets, if present, were carefully collected and weighed at the end of the 2 hr feeding period. The cages of both Ad-lib and ITAD groups were changed each day to exclude the accumulation of food particles from the preceding day. In studies involving Ad-lib fed control (Con) and tissue-specific *Atg7*KO mice, both Ad-lib fed groups (Con and KO Ad-lib groups) were pair-fed the same amount of food.

METHOD DETAILS

Autophagy Flux Assay

Autophagy/LC3-II flux was performed in freshly isolated tissues at the time-points indicated in Figure legends. Freshly collected tissue explants were incubated in dishes with high-glucose DMEM in presence or absence of lysosomal inhibitors (Lys Inh), leupeptin (200 μM) and ammonium chloride (20 mM) at 37°C, 5% CO_2 for 2 hr. For muscle flux assays, tissue explants were incubated in oxygenated CO_2-independent DMEM in presence or absence of Lys Inh, leupeptin (100 μM) and ammonium chloride (40 mM) at 37°C for 1 hr. Tissue explants were homogenized in a buffer containing protease and phosphatase inhibitors and immunoblotted for LC3 or p62. Autophagy flux was calculated by subtracting the densitometry values of LC3-II or p62 in Lys Inh-untreated from Lys Inh-treated samples (Martinez-Lopez et al., 2016).

RNA Isolation and qPCR Analyses

Total RNA was isolated using the Trizol Reagent (Invitrogen). The aqueous phase containing the RNA was loaded onto a gDNA Eliminator Spin Column (Qiagen, USA) for elimination of genomic DNA, and RNA was isolated using the RNeasy Plus kit (Qiagen) according to manufacturer's instructions. Total RNA (1 μg) was reverse transcribed into cDNA using Superscript II (Invitrogen), and quantitative RT-PCR analyses was performed using the Power SYBR Green PCR Master Mix (Applied Biosystems, UK) on a StepOne Plus Real-Time PCR System (Applied Biosystems, UK). For each gene, values were normalized to the expression of the housekeeping gene TATA-binding protein (TBP). The mRNA expression in control samples was considered as 1 and mRNA expression in experimental samples was represented as fold-change compared to expression in controls. Comparisons were only made for expression levels between the same gene in control or KO samples. All reactions were performed in triplicate. Values were expressed in arbitrary units (a.u).

Histological Analyses

The Histology and Comparative Pathology Core at the Albert Einstein College of Medicine performed the histological analyses. Paraffin-embedded sections (5 μm thick) of formalin-fixed adipose tissues and frozen sections from gastrocnemius (GA) muscle were subjected to Hematoxylin and Eosin (H/E). Sections were analyzed under a Nikon light microscope at the indicated magnification and quantified with ImageJ software (NIH, USA). Adipocyte and myocyte areas in H&E-stained sections were measured using Image J software (NIH, USA). All histological analyses were performed by individuals blinded to the treatments.

Immunohistochemistry

Adipose tissue paraffin sections were dewaxed, rehydrated, and heated in an antigen retrieval buffer (Pepsin for F4/80 staining, and Trypsin for UCP1 staining) and incubated with 0.3% H_2O_2. Nonspecific binding sites were blocked with 2% BSA + 5% Donkey serum. For immunodetection, sections were incubated for 1 hr at room temperature with either F4/80 or UCP1 antibody, and the specific staining was detected using either SuperPicture DAB Kit (Invitrogen) for UCP1 or VECTASTAIN Elite ABC HRP Kit (Vector) for F4/80. Sections were counterstained and visualized with Nikon light microscope as described above. Frozen gastrocnemius sections (10 μm thick) were blocked in M.O.M. for 1 hour and stained with the following monoclonal antibodies: BA-D5 that recognizes type 1 MyHC isoform and BF-F3 for type 2B MyHC isoform (Hybridoma Bank) and a specific Alexa-Fluo488 secondary antibody. Images were acquired with an Axiovert 200 fluorescence microscope (Carl Zeiss, Germany).

Metabolic Profiling

An ECHO (Echo Medical Systems) magnetic resonance spectroscopy instrument was used for body composition determination. Energy expenditure assessments were determined as described previously (Martinez-Lopez et al., 2013). Both Ad-lib and ITAD-fed groups were maintained on Ad-lib feeding for 3 days of acclimatization at 22-23°C followed by 5-7 days of assessments of VO_2 (oxygen consumption), VCO_2 (carbon dioxide production), EE (energy expenditure), and locomotor activity in CLAMS/metabolic cages (Columbus Instruments, USA) open-circuit indirect calorimetry.

Tissue Respirometry

Tissue bioenergetics was determined using a Seahorse respirometer (Martinez-Lopez et al., 2016). Briefly, BAT and liver were collected rapidly after sacrifice, and rinsed with Krebs-Henseleit buffer (KHB) (111 mM NaCl, 4.7 mM KCl, 2 mM MgSO4, 1.2 mM Na2HPO4, 0.5 mM carnitine, 2.5 mM glucose and 10 mM sodium pyruvate). Tissues were cut into small pieces (6-10mg) and quickly transferred to individual wells of a XF24 plate. Individual pieces were stabilized from excessive movement by islet capture screens (Seahorse Bioscience), and 450 μL KHB was added to each well. Digitonin was added to enhance plasma membrane permeability. Basal oxygen consumption rates (OCR) were determined at 37°C according to the following plan: Basal readings recorded every 2min for 10 readings, followed by exposure to digitonin. Subsequent readings were recorded after 2min mixing and 2min rest. Basal OCR values were normalized to individual tissue weights.

Vagotomy

Hepatic vagotomy (Vgx) was performed as described (Iqbal et al., 2010). Briefly, mice were anesthetized and laparotomy was performed. The stomach was exposed and the hepatic vagus nerve was identified after carefully displacing the liver. Using a cautery unit

(Geiger Medical, Iowa, USA), the hepatic vagus nerve was selectively cauterized, and the abdominal cavities of the mice were then closed. Mice that were subjected to sham surgery served as controls (Con).

Adenoviral Cre Expression

Deletion of *Atg7* in liver was accomplished by tail vein injections of 10^9 PFU of adenoviruses expressing *Cre* recombinase (Vector Biolabs, Malvern, PA, USA) and mice were humanely killed 7 days after injections. Knockdown of *Atg7* in liver was determined by immunoblotting for ATG7 and LC3.

Stromal Vascular Fraction Isolation

Minced adipose tissue samples were treated with 1 mg/mL Collagenase Type I (Worthington Biochemical Corporation) in Krebs-Ringer Buffer + 10% FCS + 1% Penicillin/Streptomycin + 2% BSA, and incubated at 37°C for 60 min. Dispersed cells were centrifuged at 500 g for 5 min. The precipitated cells from stromal vascular fractions were centrifuged at 500 g for 5 min and resuspended in DMEM supplemented with 10% FCS and 1% Penicillin/Streptomycin twice. Total mRNA was extracted from pelleted fractions as described above.

Glucose Tolerance Test (GTT)

Overnight fasted mice were administered 2 g/Kg D-glucose by intraperitoneal (i.p.) injection and blood glucose levels were measured before the injection and at indicated time-points post-injection using an Ascensia Contour glucometer (Bayer).

Pyruvate Tolerance Test (PTT)

PTT was performed as displayed in plan in Figure 4D. Mice fasted after 10am were refed for 10min at 5pm. At 6pm, 1.5 g/kg body wt of pyruvate was administrated by i.p. injection. Blood glucose levels were measured immediately prior to injection and at indicated time-points post-injection using an Ascensia Contour glucometer.

Biochemical Analyses

Serum Insulin (ALPCO, NH, USA), leptin (SPI Bio Montigny le Bretonneux, France), and FGF21 (R&D Systems, MN, USA) levels, and serum and liver triglyceride content (Sigma Aldrich, USA) were assessed using commercial kits according to manufacturer's instructions.

Western Blotting

Total protein from tissues was isolated in buffer containing 20 mM Tris, pH 7.5, 1% Triton X-100, 1 mM EDTA, 1 mM EGTA, and protease/phosphatase inhibitors. Total protein from adipose tissue was isolated by homogenization in RIPA buffer containing 50 mM Tris, 150 mM NaCl, 1% NP-40, 0.5% sodium deoxycholate, 0.1% SDS, 0.1 mM EDTA, 0.1 mM EGTA, and protease/phosphatase inhibitors. Lysates were centrifuged and supernatants were subjected to immunoblotting by denaturing 20-50 μg of protein at 100°C for 5 min in Laemmli sample buffer containing 62.5 mM Tris, 2% SDS, 25% glycerol, 0.01% bromophenol blue, and 5% β-mercaptoethanol. Samples were resolved on SDS-PAGE and transferred to nitrocellulose membranes (GE Healthcare, USA) in transfer buffer containing 25 mM Tris, 192 mM glycine, 0.01% SDS, and 15% methanol using a Bio-Rad semidry transfer cell at 150 mA for 90 minutes. Membranes were blocked in 5% nonfat dry milk, 20 mM Tris, 500 mM sodium chloride, and 0.5% Tween-20 for 1 hr and probed with primary antibodies.

QUANTIFICATION AND STATISTICAL ANALYSIS

NIH ImageJ software (Bethesda, MD, USA) was used to quantify myocyte and adipocyte size in tissues from Ad-lib and ITAD-fed mice in a blinded manner. Statistical analyses were carried out by GraphPad Prism 6 Software (GraphPad Software; La Jolla, CA, USA). Statistical details for each experiment including n value and the number of male and female mice per experiment are provided in the Figure legend. We performed the Shapiro-Wilk test to determine the normal distribution of the variables being tested. All data are mean ± s.e.m., and from a minimum of three independent experiments unless otherwise stated. Statistical significance was compared by two-tailed unpaired Student's t-test when two groups were compared, or One or Two-Factor ANOVA followed by Bonferroni multiple comparison test when multiple comparisons were made. $^*P<0.05$, $^{**}P<0.01$, $^{***}P<0.001$.